A TALE OF TWO COBALTS

Thesis by

Stephanie M. Laga

In Partial Fulfillment of the Requirements for the

degree of

Bachelor of Science

CALIFORNIA INSTITUTE OF TECHNOLOGY

Pasadena, California

2014

(Defended June 6, 2014)

ACKNOWLEDGEMENTS

I wish to express my deepest gratitude to Harry B. Gray for welcoming me into his group and helping me to explore my interests in chemistry. Doing undergraduate research in Harry's lab was my most positive experience at Caltech. Being a part of his Solar Army has provided me with countless opportunities to grow personally and intellectually. Harry's genuine enthusiasm has inspired me to pursue inorganic chemistry in graduate school, working on science that fosters a more sustainable future.

I also am very grateful to the two postdoctoral mentors who provided me with constant support and invaluable advice. I started working with Smaranda Marinescu as a sophomore when I first declared chemistry. Her patience and enthusiasm for mentoring made my first lab experience wonderful. Working with James D. Blakemore has been an immense honor. Not only does he have stellar ideas, but he also spices up lab with Swiss Radio and awesome catchphrases - "It's going to be great!"

It has been my pleasure to work with the exceptional members of the Gray group and the Caltech community. I offer many thanks to Jay Winkler and Bruce Brunschwig for help and advice on my projects and to Douglas Rees for coordinating senior thesis. I also am grateful for help with crystal structures from Larry Henling, Aaron Sattler, and Michael Takase, GCMS from Jie Zhou, and NMR from David VanderVelde.

Lastly, I would like to thank a few people who personally supported me in my studies. My time at Caltech was made so much more enjoyable by fellow chemist Iva Rreza, a great peer and dear friend. Finally, I wish to express love and thanks to my family and closest friend Jenny Yu.

This work has been supported in part by the Caltech SURF program, the National Science Foundation (NSF) Center for Chemical Innovation in Solar Fuels, and a grant from Chevron-Phillips.

ABSTRACT

There are important problems to overcome if solar energy or other renewable energy sources are to be used effectively on a global scale. Solar photons must not only be harvested and converted into a usable form, but they must also be efficiently stored so that energy is available for use on cloudy days and at night. In this work, both the energy conversion and energy storage problems are addressed. Specifically, two cobalt complexes were designed and their reactivity probed for applications in energy conversion and storage.

The first chapter describes a cobalt complex that is the first example of a dimeric cobalt compound with two singly proton-bridged cobaloxime units linked by a central BO_4^--bridge. The compound was prepared from the well-known proton-bridged cobaloxime complex and trimethoxy boron under anhydrous conditions. Single crystals of the compound suitable for X-ray diffraction studies were obtained, and confirmed the structure of the dimer. Using electrochemical methods, the redox properties of the dimer were evaluated and it was found to be an electrocatalyst for proton reduction in acetonitrile.

Because hydrogen gas is difficult to handle and store, the hydrogenation of CO_2 and later dehydrogenation of the liquid product, formic acid, has been proposed as a hydrogen storage system. Thus, a second complex supported by a triphosphine ligand framework, described in Chapter 2, was used as a catalyst precursor for this key dehydrogenation step. The studies here demonstrate the efficacy of the complex as a precatalyst for the desired reaction, with good conversion of starting formic acid to CO_2 and H_2.

In order to better understand the properties of the triphosphine cobalt complex, a synthetic procedure for substituting electron donating groups (e.g., methoxy groups) onto the ligand was investigated. A novel diphosphine cobalt(II) complex was obtained and its structure confirmed by X-ray crystallography. The redox properties of this compound were studied by cyclic voltammetry, and are compared with the parent triphosphine.

TABLE OF CONTENTS

LIST OF FIGURES AND SCHEMES

Figure *Page*

Figure (continued) *Page*

Scheme ..... *Page*

LIST OF EQUATIONS AND TABLES

Equation *Page*

Table *Page*

NOMENCLATURE

CV. Cyclic voltammetry.

DMF. Dimethylformamide.

dmg. Dimethylglyoxime.

dpg. Diphenylglyoxime.

DPV. Differential pulse voltammetry.

HER. Hydrogen evolution reaction.

IVCT. Intervalence charge transfter.

KIE. Kinetic isotope effect.

MeCN. Acetonitrile.

OEC. Oxygen-evolving complex.

PEMFCs. Proton-exchange membrane fuel cells.

py. Pyridine.

SCE. Saturated calomel electrode.

Triphos. 1,1,1-Tris(diphenylphosphinomethyl)ethane.

Chapter 1

HYDROGEN EVOLUTION WITH A NOVEL BO_4^--BRIDGED COBALT GLYOXIME DIMER

Introduction

The world's growing population continues to demand more and more energy. These needs are met currently by fossil fuels; however, it is essential to find clean and sustainable alternatives due to the risks of anthropogenic climate change. Many energy technologies discussed today, including natural gas and nuclear fission power plants, wind turbines, and carbon capture facilities, to name a few, may provide relief from the overuse of fossil fuels like oil and coal. Nonetheless, the most promising long-term option appears to be solar energy, due to its abundance and exploitability. Given that the sun provides more energy to the earth in one hour than is consumed by humans in one year,[1] its potential as an energy provider is remarkable, especially since solar energy represents a carbon-free energy source.

Water splitting is an attractive approach for storing the energy of sunlight, solar photons, and converting them into stored chemical energy. Nature has been splitting water for billions of years in a process called photosynthesis, in which water undergoes a light-driven four-electron oxidation to dioxygen. The liberated protons and electrons can then be used to form hydrogen gas. Briefly, excitation of a chlorophyll molecule by light initiates electron transfer from Photosystem II to Photosystem I. Four electrons and four protons are used to reduce nicotinamide adenine dinucleotide phosphate ($NADP^+$) to form NADPH, which is then used by plants as "fuel" for their cellular processes. To provide the electrons needed for NADPH production, H_2O is oxidized at the manganese cluster of the oxygen-evolving complex (OEC).

$$\text{Oxidation:} \quad 2H_2O \rightleftharpoons O_2 + 4e^- + 4H^+ \qquad (1.1) \qquad E^o = 1.23\ \text{V}$$

$$\text{Reduction:} \quad 4e^- + 4H^+ \rightleftharpoons 2H_2 \qquad (1.2) \qquad E^o = 0.00\ \text{V}$$

$$\text{Overall:} \qquad 2H_2O \rightleftharpoons O_2 + 2H_2 \qquad (1.3) \qquad E^o = 1.23\ V$$

Of the two half-reactions occurring in water splitting, as shown in Equations 1.1-1.3, the oxidation of water to oxygen is more energetically demanding than proton reduction.[2] The OEC accomplishes this task by using a structurally complex cluster, consisting of four manganese (Mn) ions, a calcium (Ca^{2+}) ion, and a chloride (Cl^-) ion. Three of the manganese are arranged into a cuboid structure, while the fourth manganese ion is attached to the outside of the cuboid by a bridging oxide ion.[3] While the Ca^{2+} cation can be replaced by some other metal Lewis acids, the OEC will not function if Mn is replaced by other first-row transition metals. The necessity for Mn seems to be based on the high rates of water exchange for Mn^{2+} and the ability of Mn to reach a wide range of oxidation states, especially Mn(III) and Mn (IV).[4] The precise structure of the OEC is not known and continues to be investigated,[5–7] leading to difficulties in elucidating the exact mechanism employed for water oxidation. Nonetheless, two different proposals for O–O bond formation have emerged: oxidative coupling between bridging bis-μ-oxo ligands and nucleophilic attack of H_2O or OH^- on a terminal oxo species.[3]

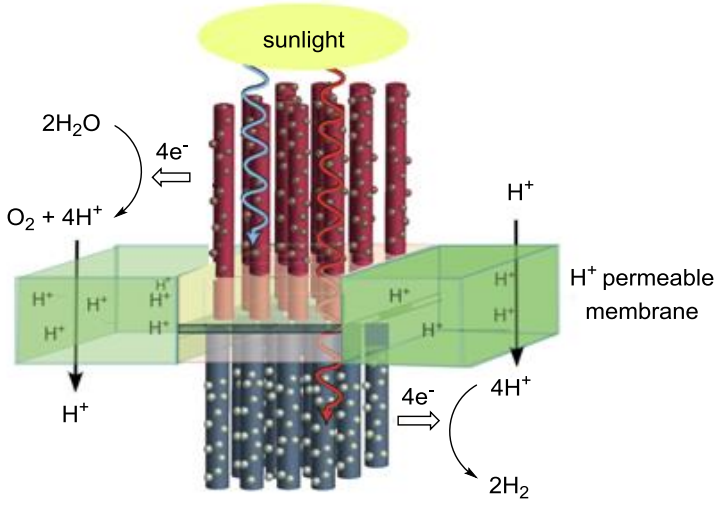

Figure 1.1. A model device architecture for water splitting. The process of interest is electrochemical proton reduction ($4e^- + 4H^+ \rightarrow 2H_2$) as shown on the lower, photocathode component.

Great progress has been made on the reductive side of water splitting, namely the hydrogen evolution reaction (HER) (Equation 1.2). Dihydrogen evolution is of particular interest because of hydrogen's value as a clean and renewable fuel.[1,8–10] In particular, hydrogen production by (photo)electrochemical proton reduction represents a viable pathway to clean fuel generation using renewable energy sources (Figure 1.1). Because many (photo)electrode materials are inherently poor catalysts for hydrogen production, the development of catalytic molecules and materials has received great attention in recent years.

While platinum is the best catalyst for hydrogen evolution, the metal's scarcity and high cost limit its use. In order for platinum to be an effective resource for energy harvesting and conversion, it would have to be able to scale to the terawatt level: Proton-exchange membrane fuel cells (PEMFCs) would require some 300 tons of platinum for 1 TW of power, a statistic made all the more staggering given that society consumes roughly 16 TW of power globally.[11] As a result, there has been great interest in catalysts that make use of earth abundant metals like nickel,[12–15] cobalt,[16–19] iron,[20] and molybdenum[21].

In terms of heterogenous systems for hydrogen evolution, two promising systems have emerged: nickel-molybdenum and cobalt-phosphide. Progress on nickel-molybdenum (Ni-Mo) alloys gained momentum in the 1980s when Ni-Mo cathodes were shown to be extremely active and stable, with overvoltages of about 60 mV over 11,000 hours of electrolysis.[22] Previously, Ni-Mo alloys were applied directly to electrodes or substrates, but current work has lead to the development of methods for depositing Ni-Mo on silicon surfaces (photocathodes)[23] and synthesizing unsupported Ni-Mo nanopowders.[24] However, Ni-Mo is only stable under strongly alkaline conditions.

Popczun, Roske and co-workers have overcome this problem with their report of cobalt phosphide (CoP) nanoparticles as an electrocatalyst for HER under acidic conditions with an overpotential (-85 mV for a current density at -20mA cm^{-2}) that compares well to the those of other HER eletrocatalysts.[25] These include Ni_2P,[26] Mo_2C on carbon nanotubes,[27] and MoS_2,[28] with overpotentials that range from -130 to -175 mV. While the CoP

nanoparticles system has about the same overpotential as Ni-Mo (-80 mV),[23] the CoP system may be considered more advantageous due to its stability in strongly acidic conditions.

Molecular catalysts can also be immobilized on electrode surfaces (Figure 1.2). Berben and Peters reported aryl-substituted tetraimine cobalt complexes, analogues of a $Co(dmgBF_2)_2(MeCN)_2$ cobaloxime that readily adsorbed on a glassy carbon electrode.[29] Alternatively, Krawicz et al. functionalized a p-type gallium phosphide surface with polyvinylpyridine which subsequently could bind a cobaloxime catalyst for hydrogen evolution.[30] Fontecave and Artero attached a cobaloxime to a carbon nanotube electrode using a diimine-dioxime ligand, although clear comparisons with the analogous soluble compound under the assayed conditions were not provided.[31] Thus, it remains of interest to develop new synthetic routes for proton-reduction catalysts, since more complex ligand architectures can be used to tether catalysts to surfaces or to generate multimetallic species with novel reactivity.

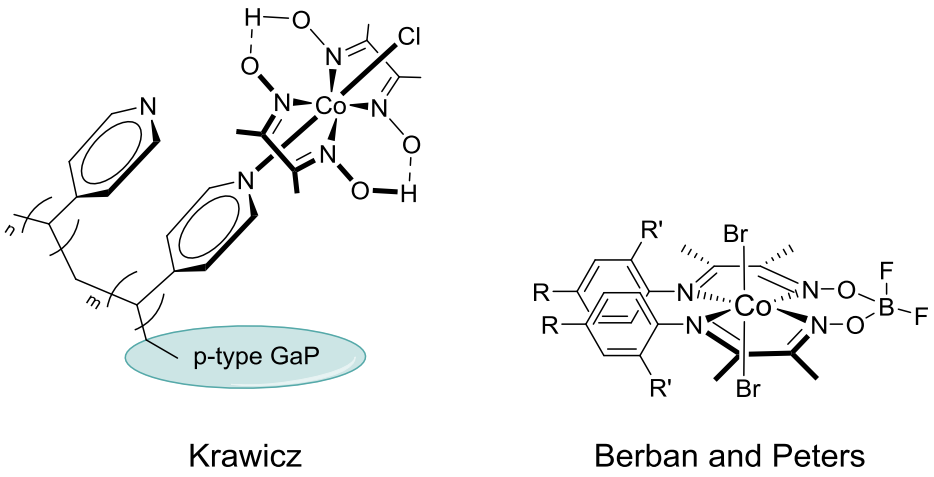

Figure 1.2. Selected examples of immobilized HER catalysts.

Great progress has been made on developing homogeneous HER catalysts using a variety of earth-abundant transition metals (Figure 1.3). Dubois reported a series of monomeric nickel phosphine complexes that reduced dimethylformamide with extraordinary turnover frequencies as high as 106,000 s^{-1} in a solution of 1.2 M water in acetonitrile.[12]

Alternatively, a molybdenum-oxo complex with a pentadentate pyridine ligand was described as a precatalyst for hydrogen generation in water.[21] Closely related are a set of cobalt compounds, also featuring the pentapyridine ligand, that generate hydrogen electrochemically with a mercury electrode in aqueous solutions, [32, 33] with a $[Ru(bpy)_3]^{2+}$ photosensitizer in aqueous solutions,[34] or under diffusion limited conditions in acetonitrile.[35] In older work, Kölle and Grätzel demonstrated the photoreduction of protons on a TiO_2 colloid using rhodium(III) catalysts that were reduced at a potential of -0.75 V vs. SCE.[36]

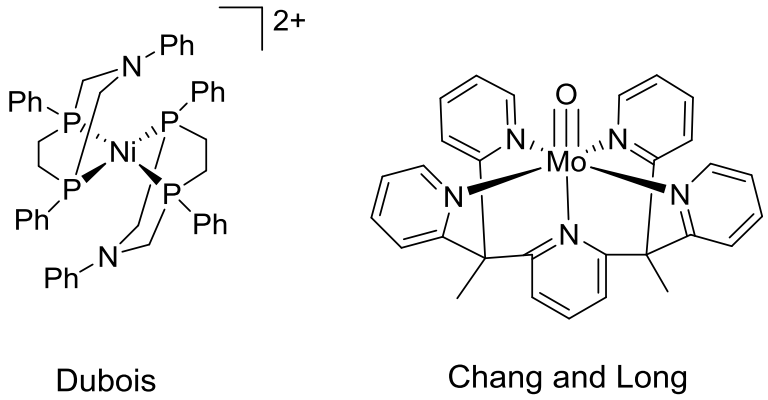

Figure 1.3. Selected homogeneous HER catalysts.

Cobalt glyoxime complexes have also been extensively studied in the context of hydrogen evolution (Figure 1.4). These complexes gained attention after Schrauzer's work with cobaloxime derivatives as mimics of vitamin B_{12}.[37] Soon after the first cobalt glyoximes, were isolated by Shrauzer and Holland, work began on the elucidation of their mechanistic importance in the evolution of hydrogen by Spiro[38] and Espenson, who found $Co^{II}(dmgBF_2)_2(H_2O)_2$ could reduce protons in aqueous conditions.[39] In acetonitrile with acid sources, the BF_2-bridged cobaloximes, $Co^{II}(dmgBF_2)_2(MeCN)_2$[16] and $Co^{II}(dpgBF_2)_2(MeCN)_2$,[40] were shown to reduce protons at -0.55 V vs. SCE and -0.28 V vs. SCE respectively. It was found that the potential at which hydrogen is evolved is correlated, unsurprisingly, with the electronic properties of the ligand. A compound with

weaker electron donating ligands will be more easily reduced and, hence, evolve hydrogen at a more positive potential.[18]

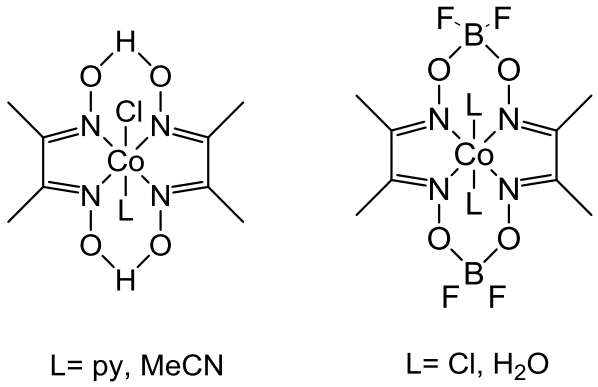

Figure 1.4. Proton and difluoroborate-bridged cobaloximes.

In addition to these mononuclear complexes, di-iron and nickel-iron hydrogenase mimics have garnered attention. In biological systems, hydrogenase enzymes containing iron (Figure 1.5) and nickel cofactors can produce dihydrogen from water at the thermodynamic potential with turnover frequencies as high as 9000 s^{-1} at 30 °C.[41, 42] Thus, mimics are especially interesting because they imitate the natural structure of protein active sites.[43–46]

However, the hydrogenases are unstable in aerobic environments and easily degraded by competing side chemical processes. It is generally thought that these mimics tend to function poorly since they are no longer surrounded by their natural protein environment.[9, 47]

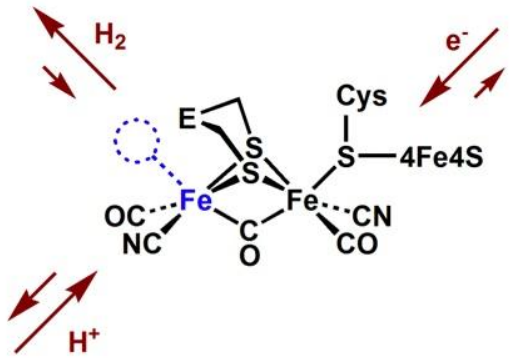

Figure 1.5. Model of the active site of hydrogenase.

Development of multinuclear catalysts has also been of recent interest, as multiple sites may promote reactivity that is not accessible with a single site. Enhanced reactivity by dimeric complexes, in comparison to monomeric complexes, has also been demonstrated in several hydrogen evolving catalysts.

In 1992, Collman et al. reported a series of ruthenium and osmium cofacial bisorganometallic diporphyrins that evolve hydrogen in the presence of acid.[48] They attempted to make use of the cofacial orientation of the porphyrins to facilitate dinuclear H_2 elimination. Although catalysis was not as rapid as expected, electrochemistry on a mercury-pool electrode demonstrated that the cofacial bimetallic system was more stable than its monomeric analogue.[49]

At Caltech, Peters and coworkers reported bimetallic analogues of various difluoroborate-bridged cobaloximes (Figure 1.6) with the ability to reduce protons at low overpotentials. Electrochemical studies of these dicobalt compounds revealed two nicely separated Co(III/II) couples and also two resolved Co(II/I) couples, indicating stability of the mixed valence intermediates. The potentials of the redox events ranged from -0.30 to 0.18 V vs. SCE for the $Co^{II}Co^{II}/Co^{II}Co^{I}$ and $Co^{II}Co^{I}/Co^{I}Co^{I}$ couples and 1.07-1.35 V vs. SCE for the $Co^{II}Co^{II}/Co^{II}Co^{III}$ and $Co^{II}Co^{III}/Co^{III}Co^{III}$. It is also of note that these complexes exhibited IVCT bands consistent with a Class II-III mixed valence species according to the Robin-Day classification system. This indicates that the cobalt centers are moderately to strongly coupled.[50]

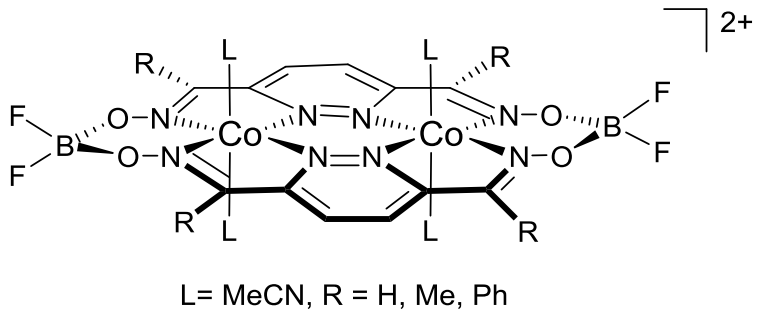

Figure 1.6. Dicobaloxime complex reported by Peters and coworkers.

Similarly, Valdez et al. published a dicobalt system with octamethylene-linked bis(glyoxime) ligands (Figure 1.7). In this system, hydrogen evolution was proposed to occur by the protonation of a reductively generated Co^{II}-H. However, electrochemical studies revealed no enhancement of electrocatalytic hydrogen evolution rates over the mononuclear analogue.[51]

Cobalt complexes bearing proton-bridged or BF_2-bridged dimethyl or diphenyl glyoxime ligands were found many years ago to be suitable catalysts for reduction of protons to dihydrogen, but synthetic methods remain elusive for generating multinuclear compounds or structures amenable to immobilization on electrodes. We have been investigated a new synthetic pathway to enable such further derivatization of these complexes.

Thus, we now report the preparation and characterization of a novel dimeric cobalt dimethylglyoxime complex that is bridged by BO_4^-. The complex was prepared by treatment of the doubly proton-bridged mononuclear glyoxime, first obtained by Schrauzer and Holland,[52] with trimethoxy boron under anhydrous conditions, yielding the novel compound. Furthermore, we have characterized its electrochemical and catalytic properties for hydrogen evolution in acetonitrile.

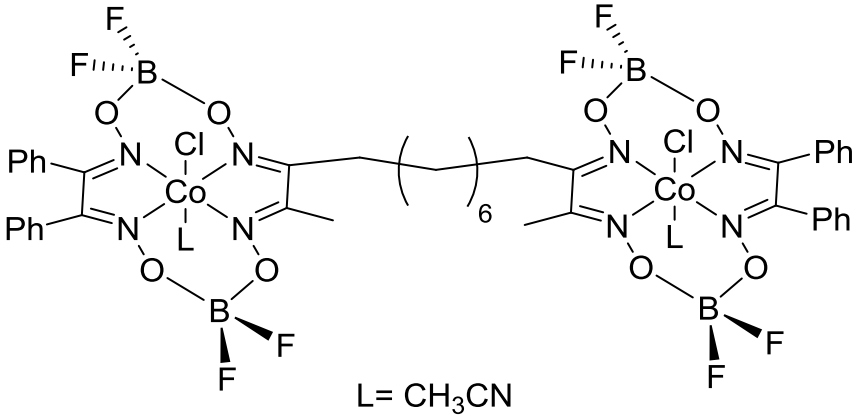

Figure 1.7. Dicobaloxime complex reported by Valdez et al.

Synthesis of a BO_4^--Bridged Dimeric Cobaloxime Complex

Synthesis of the dimeric cobaloxime was accomplished in two steps (Scheme 1.1). Starting from cobalt(II) chloride hexahydrate and dimethyl glyoxime, the green monomeric proton-bridged cobaloxime, $[Co^{III}(dmgH)_2(MeCN)Cl]$ (dmg=dimethylglyoximate), was obtained as described in the procedure by Grimes without the addition of pyridine.[53] This complex is air stable and appears brown upon addition of pyridine. The pyridine cobaloxime adduct, $Co^{III}(dmgH)_2(py)Cl$ (py=pyridine), exhibits a reversible $Co^{II/I}$ couple at -0.98 V vs Ag/AgCl and an irreversible $Co^{III/II}$ couple at -0.59 V vs Ag/AgCl.[54]

Treatment of this proton-bridged glyoxime compound with trimethyl borate and tetramethylammonium chloride in MeCN gave a new BO_4^--bridged dimer of singly H^+-bridged cobalt(III) glyoxime units. Recrystallization in acetonitrile with ethyl ether yields the species as brown crystals.

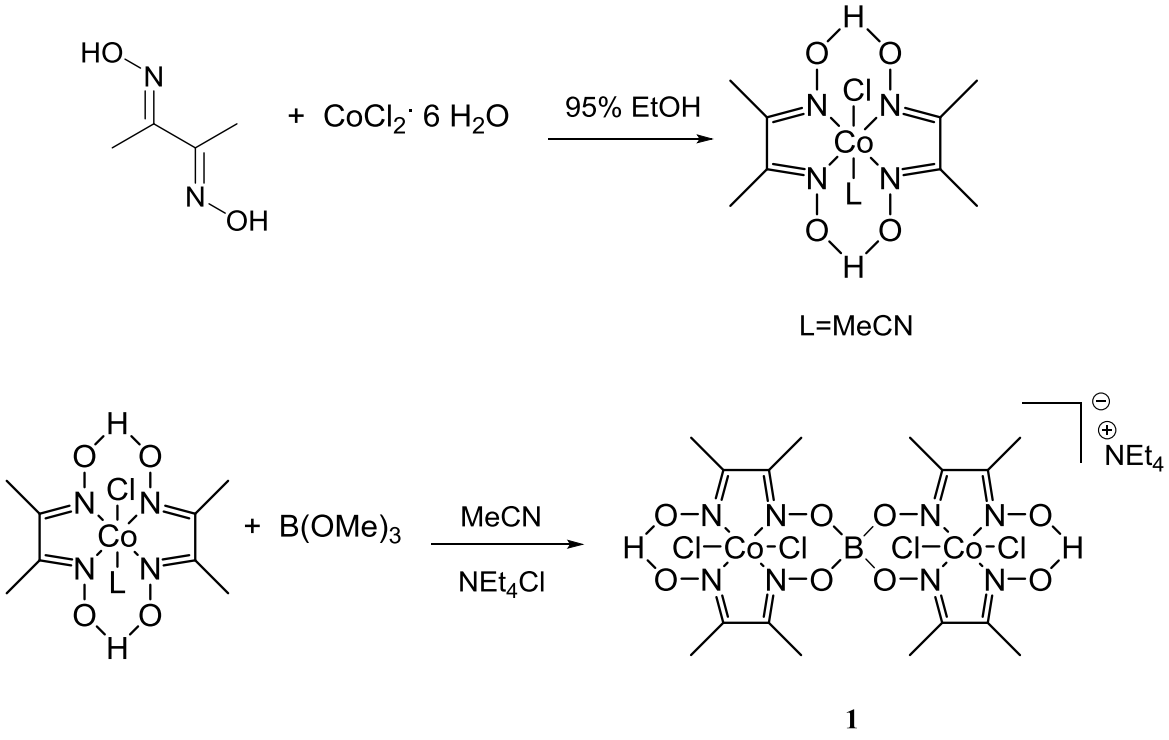

1

Scheme 1.1. Synthesis of the novel BO_4^--bridged dimeric cobaloxime.

X-Ray Crystallography of the BO_4^--Bridged Dimeric Cobaloxime

Brown blade-like crystals of complex **2** submitted for X-ray crystallography revealed a triclinic crystal with two cobalt centers with pseudo-octahedral geometry and a bridging BO_4^- moiety with a distorted tetrahedral geometry (Figure 1.8). Each cobalt center is coordinated by two essentially planar dimethylglyoxime ligands and two chlorides in the axial *trans* positions. The observed Co-N distances are each near 1.88 Å and those of the Co-Cl bond are near 2.23 Å. The Co-N distances are comparable to those of monomeric cobaloxime complexes, with bond lengths that are often near 1.89 Å.[18]

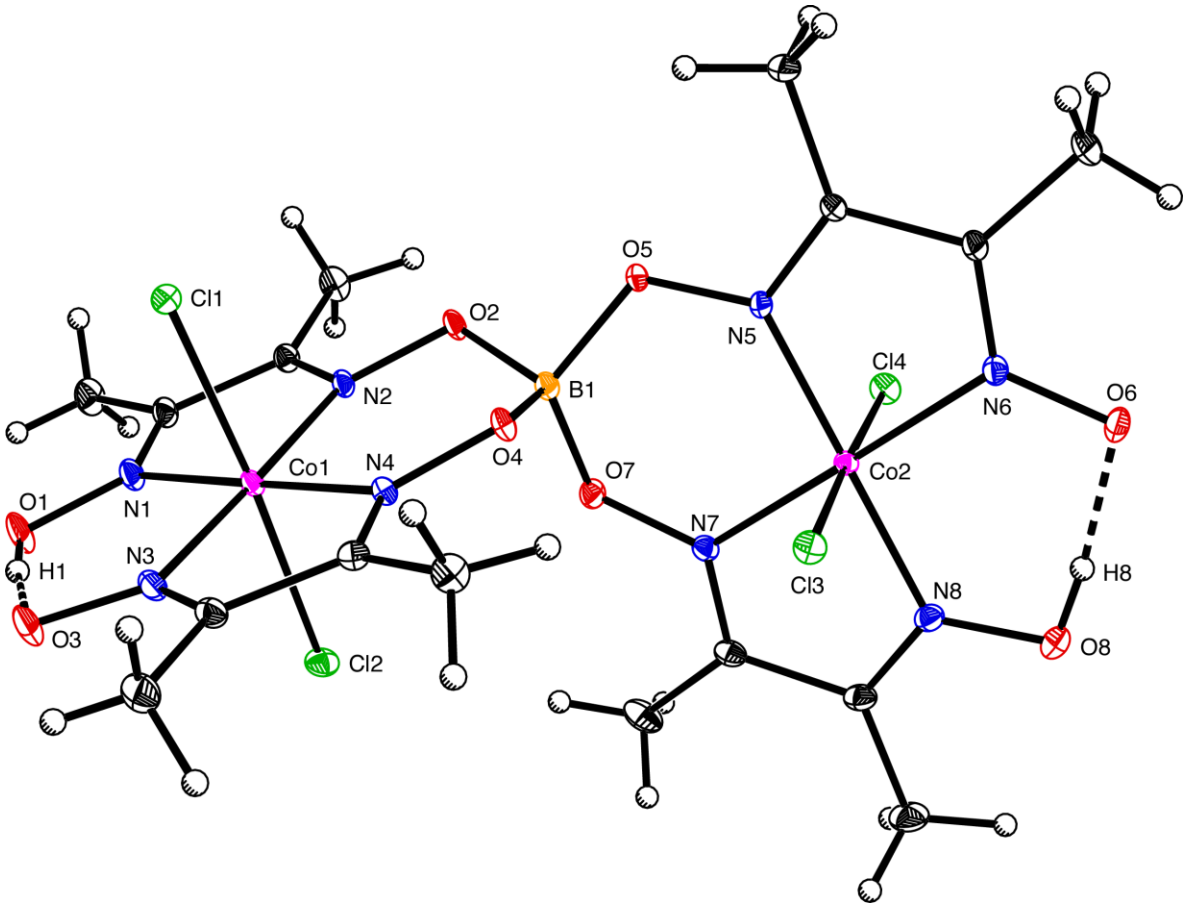

Figure 1.8. Crystal structure of the BO_4^--bridged dimeric cobaloxime.

The two cobaloxime units bridged by BO_4^- form a Co-B-Co angle of 145.21°, with an observed Co-B distance of 3.211 Å and a Co-Co distance of 6.136 Å (see Tables A1 and A2). The metal-to-metal distance is likely too large to permit IVCT. Supporting this notion, IVCT bands were not observed in the expected 700-1000 nm region during spectroelectrochemical studies of the complex. The pyridazine-bridged dicobalt complexes reported by Peters and coworkers did observe IVCT bands from about 750-900 nm,[50] but in their Co^{III}-Co^{III} compound the cobalt centers were closer at 3.798 Å.

A tetraethylammonium chloride counterion was observed to balance the -1 charge of the complex. If the counterion is omitted from consideration, C_2 symmetry is observed in the complex due to the orientation of the two large macrocycles. The distorted tetrahedral boron center prevents the macrocycles from being coplanar or cofacial. They are best described as pseudo-orthogonal. These assignments are consistent with the spectroscopy (see below).

Spectroscopic Studies of the BO_4^--Bridged Dimer

Nuclear magnetic resonance (NMR) spectroscopy of the brown crystals confirmed their purity and structure. The ^1H NMR spectrum of complex **1** (see Figure A1) exhibited a triplet and quartet at 1.22 and 3.17 ppm, respectively, for the countercation tetraethylammonium. Two singlets with a 1:1 integration appear at 2.47 and 2.56 ppm as expected for the dimethylglyoxime methyl groups. Finally, a signal was found at 18.4 ppm, attributable to the two bridging protons of the complex. In the ^{13}C NMR, six signals are observed as expected (see Figure A2), while in the ^{11}B NMR there was a singlet at 7.41 ppm (Figure 1.9). These signals provide strong evidence for the existence of the proposed structure.

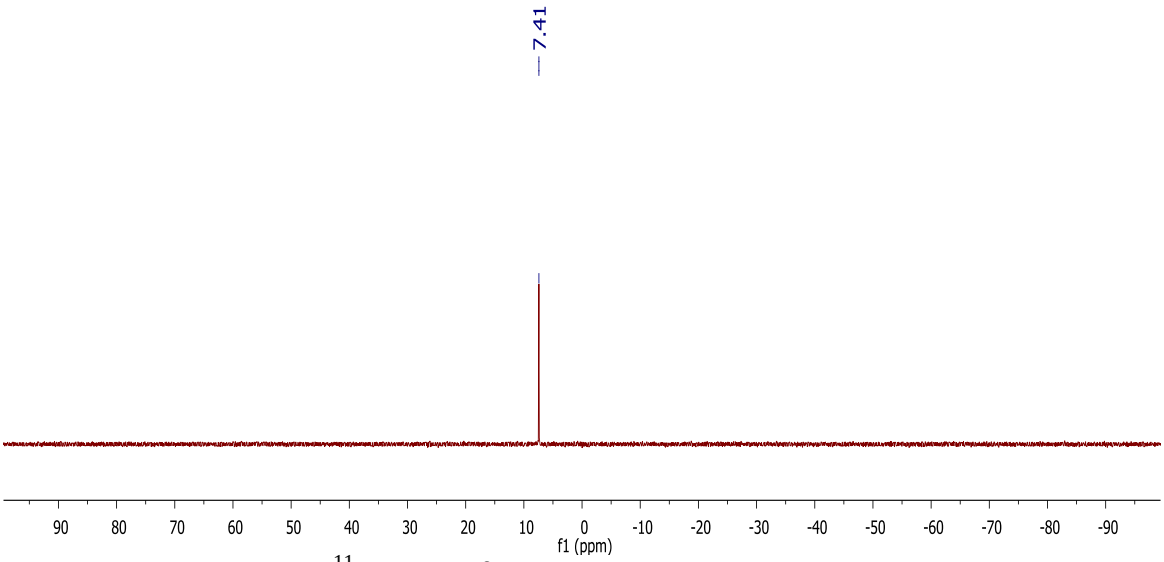

Figure 1.9. ^{11}B NMR of the BO_4^--bridged dimeric cobaloxime.

Mass spectra of complex **1** corresponded nicely to the proposed structure (Figure 1.10). The negative ion spectrum exhibited a parent peak at 727.1 m/z, corresponding to the complex (charged -1 overall) without the counter ion, [dimer-NEt_4]. Peaks at 693.1 and 657.0 m/z corresponded to the [dimer-NEt_4-Cl] and [dimer-NEt_4-2Cl-H] fragments respectively. A peak at 621.0 m/z was assigned to the [dimer-NEt_4-3Cl-H] fragment.

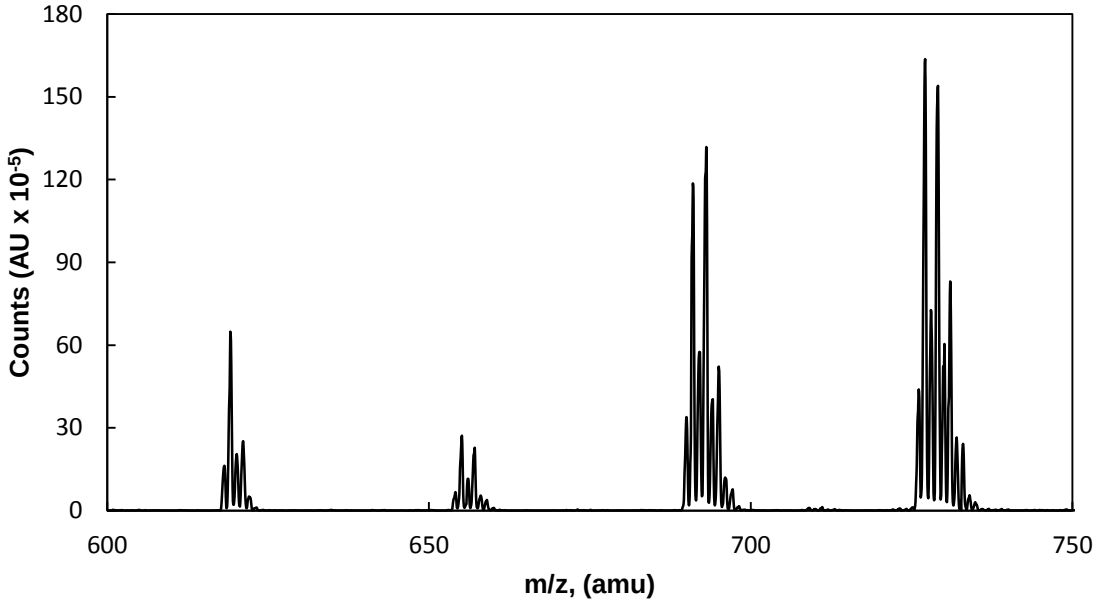

Figure 1.10. GCMS of the BO_4^--bridged dimeric cobaloxime in the negative ion phase.

Electrochemical Studies of the BO_4^--Bridged Dimeric Cobaloxime

Cyclic voltammograms collected with complex **1** using a basal-plane graphite working electrode in 0.1 M NBu_4PF_6 in MeCN show an irreversible wave at $E_{1/2}$ = –0.68 V vs $Fc^{+/0}$ which we assign to a quasi-reversible $Co^{III/II}$ couple. At more negative potentials, two closely spaced, single-electron $Co^{II/I}$ couples were observed near –1.2 and –1.3 V vs $Fc^{+/0}$ (Figure 1.11). This assignment is consistent with the bimetallic Peters system described above, which exhibited two one-electron events for each of the two paired $Co^{III/II}$ and $Co^{II/I}$ couples. In comparison, the $Co^{III/III}/Co^{III/II}$ and $Co^{III/II}/Co^{II/II}$ couples of **1** are not resolved at all from each other. Although the $Co^{II}Co^{II}/Co^{II}Co^{I}$ and $Co^{II}Co^{I}/Co^{I}Co^{I}$ one electron couples are somewhat resolved, by about 100 mV, those reported by Peters have a larger separation of about 200 mV.[50]

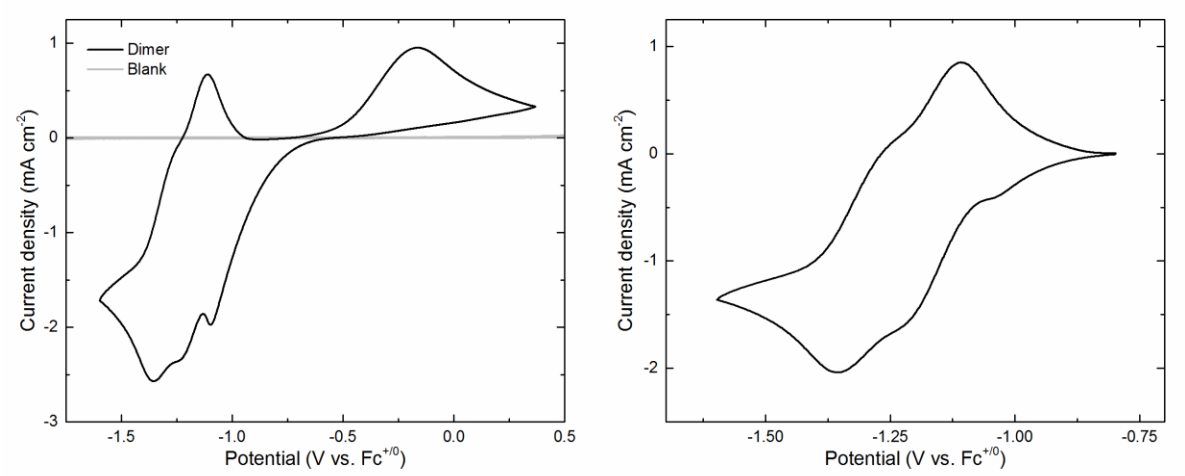

Figure 1.11. Cyclic voltammograms of the BO_4^--bridged dimeric cobaloxime. Conditions are described in the main text.

To better establish the number of electrons participating in the oxidation and reduction of complex **1**, differential pulse voltammetry was carried out using the same electrode configuration as above (Figure 1.12). Two closely spaced, but clearly resolved, signals were observed for a sample of 5 mM of the dimer in a NBu_4PF_6 acetonitrile solution, implying that two unique processes were occurring during the oxidation sweep. A reductive sweep on a 10 mM solution of ferrocenium produced a clean single peak with an area

roughly equal to that of the complex's two peak areas. The 1:1 comparison implies that indeed there is an overall two-electron process occurring as the two metal centers in the complex are oxidized from Co^{I} to Co^{II}.

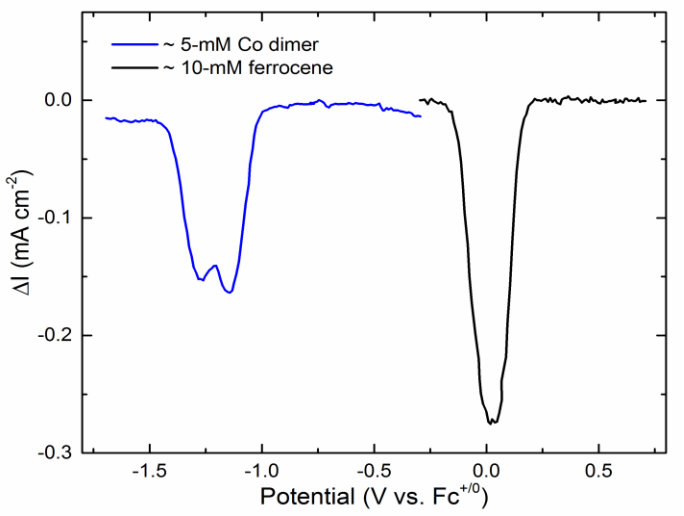

Figure 1.12. Differential pulse voltammogram of the BO_4^--bridged dimeric cobaloxime (blue line) and ferrocene (black line).

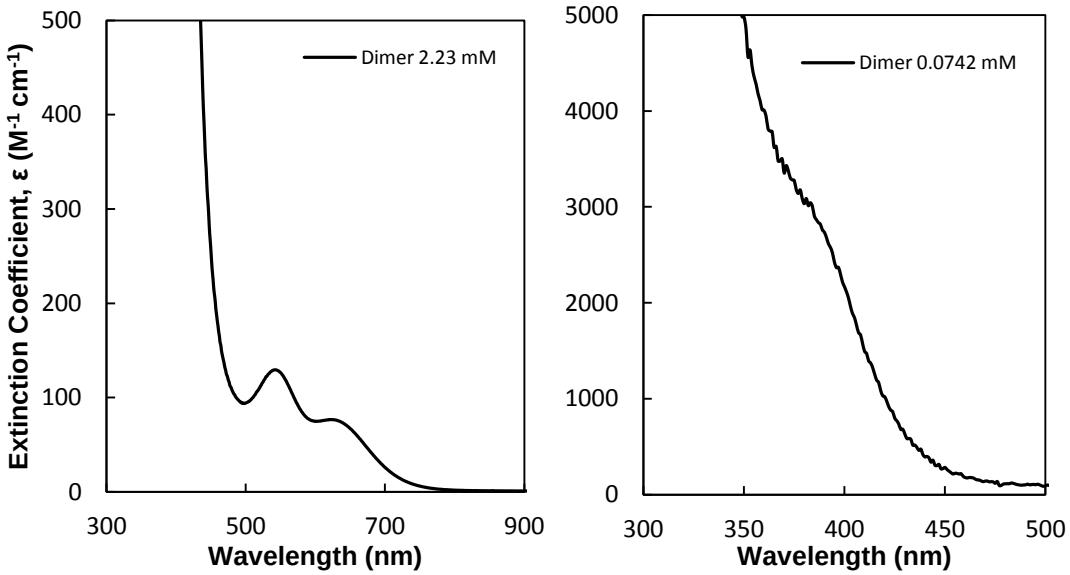

Figure 1.13. UV visible spectra of the BO_4^--bridged dimeric cobaloxime at 2.23 mM (left) and 0.0742 mM (right).

UV-visible spectrum of the BO_4^--Bridged Dimeric Cobaloxime

The UV visible spectrum of the dimer, at a concentration of 2.23 mM in acetonitrile, revealed two bands at 542 and 623 nm with extinction coefficients of 129 and 77 M^{-1} cm^{-1} respectively. At a lower concentration of 0.0742 mM, an additional band with an extinction coefficient of 3044 M^{-1} cm^{-1} could be resolved at 387 nm.

Proton-Reduction Electrocatalysis with the BO_4^--Bridged Dimeric Cobaloxime

In order to determine the ability of dimer **1** to catalyze the reduction of protons to hydrogen, cyclic voltammograms of the free dimer were compared to solutions of the dimer with increasing concentrations of an organic proton source. Specifically, we used a 1:1 solution of protonated dimethylformamide ($[DMF•H]^+$) and dimethylformamide (DMF). This buffered organic acid allows us to estimate the reversible, thermodynamic potential for the H^+/H_2 couple under these conditions; this value is -389 mV vs. $Fc^{+/0}$.[55] The data showing changes in the cyclic voltammograms upon acid addition are shown in the two panels of Figure 1.14.

The cyclic voltammetry of **1** in the presence of increasing concentrations of acid shows onset of a catalytic response near the Co(II/I) potentials of the metal complex. This is consistent with prior work on cobaloxime-catalyzed proton reduction, which shows catalytic current at similar potentials with other strong organic acids. Notably, a plateauing catalytic current was not obtained upon variation of scan rate, although the negative potentials required for catalysis precluded use of very fast scan rates due to background response complications. Thus, turnover frequencies were not calculated from the voltammetry data. However, using the method of Appel, et al., we did estimate the potential for catalysis with dimer **1** to be -1.24 V with addition of 5 equivalents of acid. This corresponds to an overpotential (under these conditions) of -850 mV. However, use of a weaker acid would likely result in similar catalysis at lower overpotential values, an area of interest for future work.

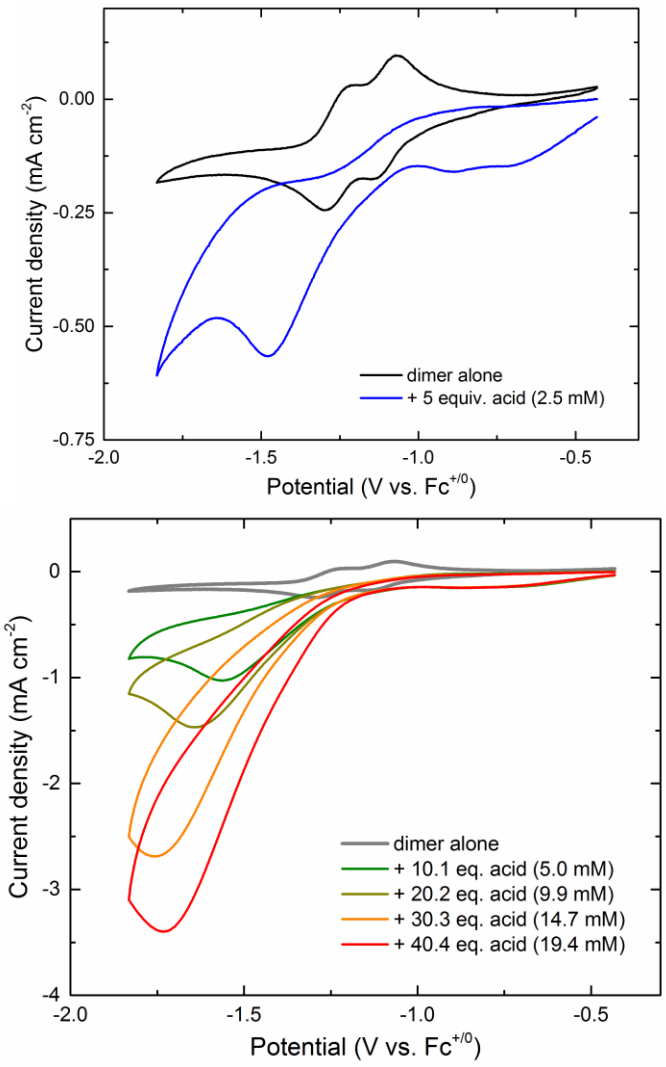

Figure 1.14. Cyclic voltammetry showing proton reduction catalysis with dimer **1** in the presence of a 1:1 $[DMF•H]^+$:DMF.

Conclusions

In summary, a new BO_4^--bridged dimeric cobalt dimethylglyoxime complex has been synthesized and fully characterized in the Co(III)/Co(III) oxidation state. The complex was synthesized by treatment of the proton-bridged mononuclear dimethylglyoxime with trimethoxy boron under anhydrous conditions. Furthermore, its electrochemical and catalytic properties have been probed for hydrogen evolution in acetonitrile, confirming that the dimeric complex can serve as an effective catalyst for proton reduction.

Chapter 2

COBALT-CATALYZED DEHYDROGENATION OF FORMIC ACID, A HYDROGEN-STORING CHEMICAL

Introduction

Despite the advancements made in the development of earth-abundant catalysts for hydrogen evolution, hydrogen's potential as a fuel on a large scale is limited by the challenge of hydrogen storage. Due to its poor energy density by volume relative to hydrocarbons, storage requires a larger tank. Energy density can be improved by pressurizing the tank, but this requires heavier tanks and significant energy for compression.[56]

Some research has focused on the storage of hydrogen in materials like carbon-based compounds, organic polymers (covalent organic frameworks), zeolites, metal-organic frameworks, clathrates and metal hydrides. These have not yet proved to be the ultimate solution to the hydrogen-storage challenge.[57]

An alternative is storing hydrogen in liquids with high hydrogen content. This route is becoming increasingly attractive because liquids can often be imagined to be transportable via existing infrastructure. In particular, formic acid is a promising liquid-storage medium, as its conversion into hydrogen and carbon dioxide is thermodynamically downhill ($\Delta G°_{298}$ = –32.9 kJ mol^{-1}) (Eqn. 2.1).[58, 59] The conversion of formic acid into H_2O and CO, is also thermodynamically downhill, but less so than dehydrogenation ($\Delta G°_{298}$ = –20.7 kJ mol^{-1}) (Eqn. 2.2).[60]. Use of carbon dioxide, an abundant and inexpensive C_1 feedstock, is also of interest because it may be used to generate HCO_2H.[55]

$$HCO_2H \rightleftharpoons H_2 + CO_2 \qquad (2.1) \qquad \Delta G^{o}_{298} = -32.9\ \text{kJ/mol}$$

$$HCO_2H \rightleftharpoons H_2O + CO \qquad (2.2) \qquad \Delta G^{o}_{298} = -20.7\ \text{kJ/mol}$$

There has been progress in developing catalysts for the hydrogenation of carbon dioxide and the decomposition of formic acid using metal complexes with noble metals.[56,60–71] Kang et al. reported the insertion of carbon dioxide into five-coordinate iridium(III) dihydride complexes with PCP-pincer ligands.[64] This is consistent with previous work performed by the Nozaki and Hazari labs, who reported similar iridium systems that reduced CO_2 to formate under basic conditions (Figure 2.1).[65–67] Alternatively, Strauss, Schriver, et al. investigated the capabilities of a rhodium(I) catalyst, $Rh(C_6H_4PPh_2)(PPh_3)_2$, to decompose formic acid to produce CO_2 and H_2. Their proposed catalytic cycle involved oxidative addition of formic acid to the complex, followed by ß-hydride elimination to produce CO_2 and an intermediate that goes on to release H_2.[69] Junge, Beller et al. investigated ruthenium-catalyzed H_2 evolution from formic acid in the presence of various amines and halide additives. It was found that more basic amidines improved catalyst performance.[71]

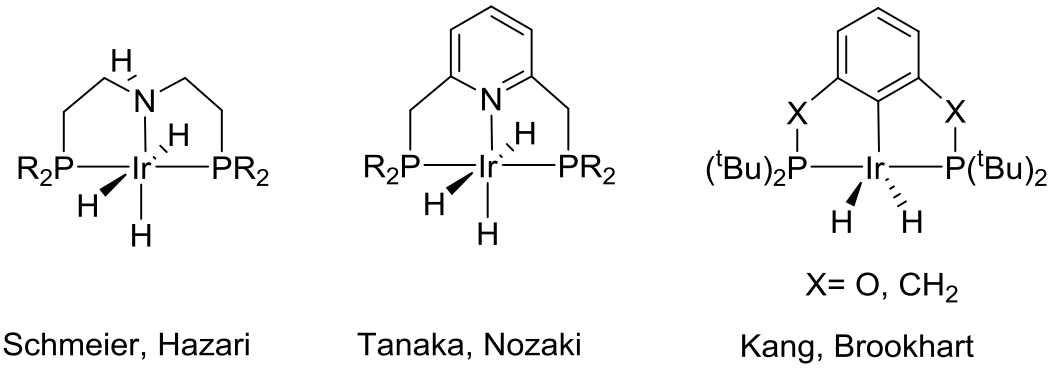

Figure 2.1. Selected noble metal catalysts that decompose formic acid.

The development of complexes that reduce carbon dioxide and selectively evolve H_2 from formic acid containing only earth-abundant metals are also known now.[72–79] Shin, Parkin et al. reported a molybdenum complex, $Cp^*Mo(PMe_3)_2(CO)H$ - formed from carbonyl abstraction reactions between $Cp^*Mo(PMe_3)_3H$ and reagents like CO_2, $(CH_2O)n$, HCO_2H, and MeOH - that catalyzes the dehydrogenation of formic acid.[72] Work by Ludwig and Beller demonstrated that formic acid could be decomposed into hydrogen and carbon dioxide using triphenylphosphine[73] and novel benzylphosphine iron catalysts that activate

via *ortho*-metalation upon irradiation with light.[74] An iron(II) complex with a pincer ligand, studied by Langer, Milstein et al., was found to catalyze the hydrogenation of bicarbonate into sodium formate with a turnover frequency of 156 h^{-1};[76] this was comparable to a study of an iron system conducted by Beller and Laurenczy, who calculated a turnover frequency of up to 30.5 h^{-1} in contrast.[75]

Federsel and Beller also demonstrate hydrogenation of CO_2 and bicarbonates with a cobalt dihydrogen complex.[78] Most impressive however is the Laurenczy, Ludwig, Beller, and coworkers iron catalyst that dehydrogenated a solution of formic acid in propylene carbonate with no further additives with a turnover frequency of up to 9425 h^{-1} (Figure 2.2).[79]

This provided the inspiration for the work completed here - investigation of a hydrogen storage system based on formic acid using a cobalt catalyst.

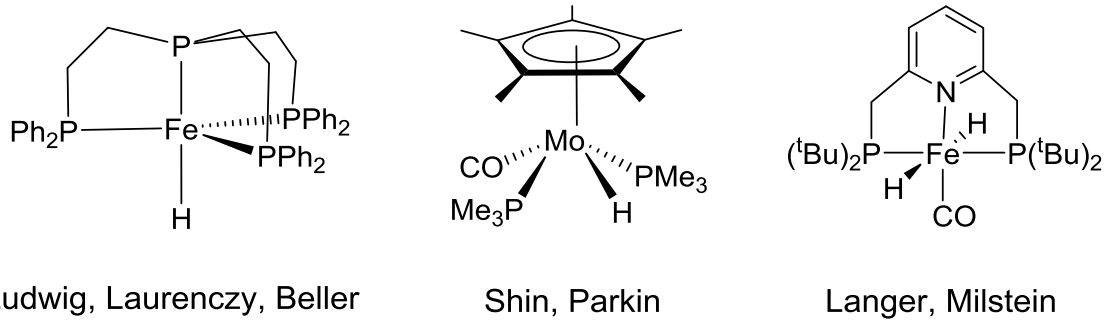

Figure 2.2. Selected earth abundant catalysts that dehydrogenate formic acid.

Cobalt Triphosphine Systems

The triphos ligand framework (triphos = 1,1,1-tris(diphenylphosphinomethyl)ethane employed here allows for facile tuning of reduction potentials because the aryl groups can be functionlized with electron-withdrawing or electron-donating groups. In 1975, Sacconi published early work in this area involving a cobalt triphos amine complex.[80] Other early work by Mealli included the synthesis and structural characterization of cobalt triphos complexes.[81] More recently, in 1997, Heinze et al. reported a set of dimeric mixed valence

cobalt triphos compounds with a benzoic system bridging ligand.[82] In addition to these examples, many more Co(triphos) species have been reported (Figure 2.3).[83] The protonation of $[(PP_3)CoH]$[84] (PP_3 = $P(CH_2CH_2PPh_2)_3$) led to the formation of a dihydride complex, $[(PP_3)Co(H)_2][PF_6]$.[85] Although $[(triphos)Co^{III}(H)_2]^+$ species have been synthesized,[86, 87] catalytic proton reduction has not been reported.

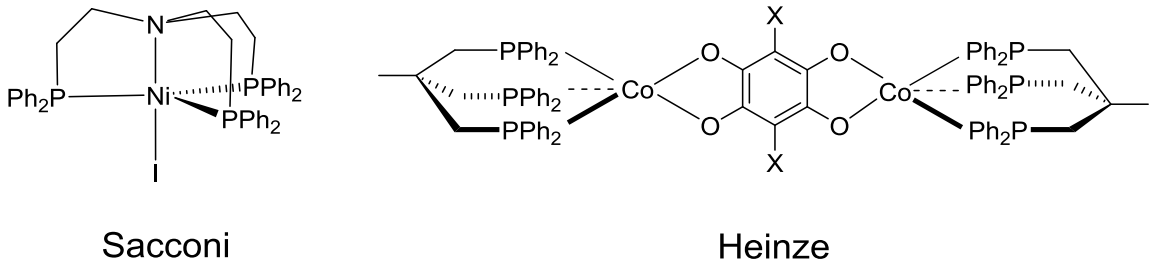

Sacconi Heinze

Figure 2.3. Selected triphos ligand catalysts.

Previous work in the Gray group has focused on a series of cobalt complexes supported by the triphos ligand framework. Cobalt(II) iodide spontaneously reacts with phosphine, yielding a pink solid, Co(triphos)(I) **(1)**.[88] When this pink solid is abstracted with $TlPF_6$ in in 5:1 THF:MeCN, a cationic acetonitrile adduct, $[Co(triphos)(MeCN)][PF_6]]$ (**2**), is generated as blue crystals. Complex **2** was found to react at room temperature with *p*-toulenesulfonic acid monohydrate to generate a half equivalent of hydrogen and cobalt(II) (Scheme 2.1).[89] In addition, CVs of **2** at a glassy carbon electrode in a 0.1 M acetonitrile solution of $[n Bu_4N][PF_6]$ revealed a reversible wave at $E_{1/2}$ = –0.68 V vs $Fc^{+/0}$ assigned to the $Co^{II/I}$ couple, and an irreversible oxidation at +0.66 V vs $Fc^{+/0}$, assigned to the $Co^{III/II}$ couple.[89]

Mechanistic work using this cobalt(I) complex (**2**), revealed that protonation produces a diamagnetic Co^{III}–H complex (**3**) that was characterized by ^1H and ^{31}P NMR spectroscopy. Complex **3** was found to be a transient intermediate that was readily reduced by Co^I to generate a reactive Co^{II}-H intermediate.[89] As such, we became interested in exploring the hydrogen evolution reaction of the cobalt system (**2**) in the presence of other acids, including formic acid.

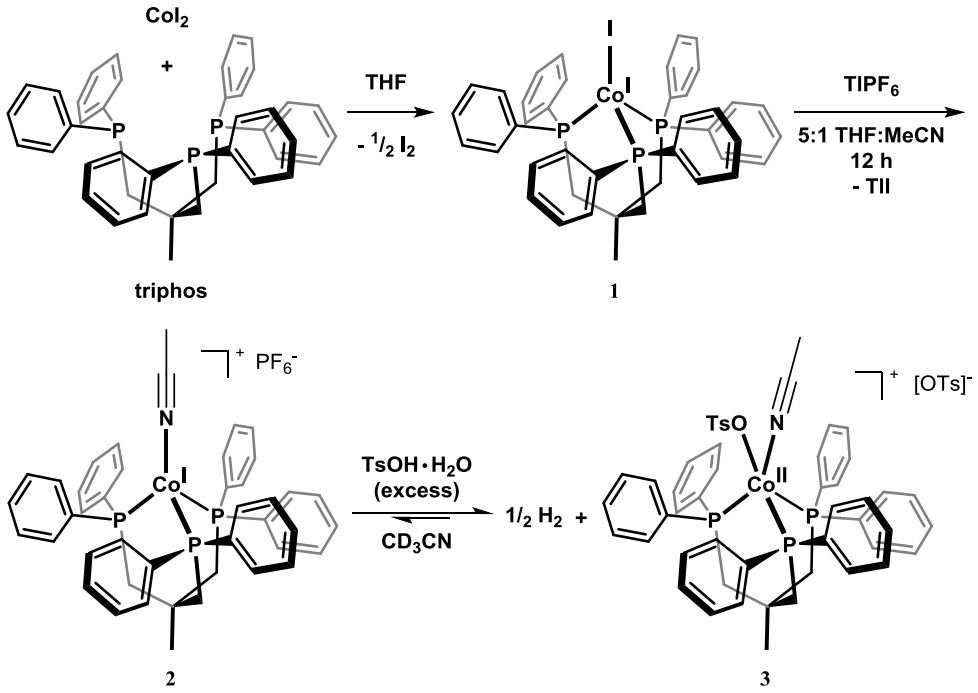

Scheme 2.1. Syntheses of cobalt(I) species.

Dehydrogenation of Formic Acid

To determine that the catalyst was in fact decomposing formic acid, the generation of H_2 and CO_2 were verified. First, the heating of formic acid (10 equivalents) and a solution of $[Co(triphos)(MeCN)]^+$ (**2**), in CD_3CN at 70 °C for four hours, led to the appearance of a singlet in the mixture's ^1H NMR at δ 4.58 ppm, signifying the presence of hydrogen gas. When this experiment was repeated in a Schlenk flask at 70 °C and stirred for 12 hours, gas chromatography indicated that 9 equivalents of hydrogen had evolved. Note that for all measurements, the mixture was placed in an oil bath at the desired temperature and allowed to equilibrate for 10 minutes. A control experiment without catalyst showed a negligble amount of gas evolution during the equilibration time. The following kinetics plots show the evolution of gases following the 10-minute equilibration time.

Second, in a separate experiment, a reaction mixture containing 10 equivalents of $H^{13}CO_2H$ in a solution of **2** in CD_3CN was heated for 2 hours at 70 °C. The presence of a singlet in ^{13}C NMR spectrum of the reaction mixture at δ 125.9 ppm indicated the formation of $^{13}CO_2$

(Figure 2.4). CO was not detected by ^{13}C NMR or gas chromatography in the reaction mixture.

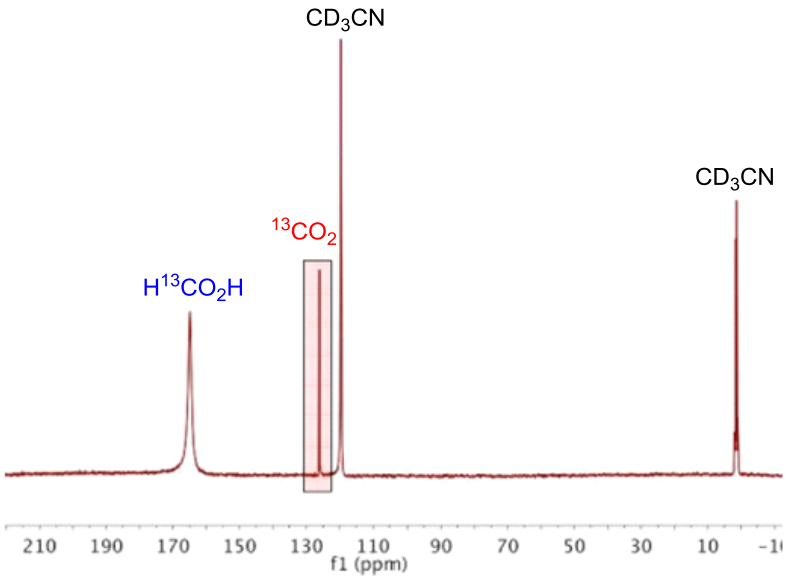

Figure 2.4. ^{13}C NMR spectrum of the reaction mixture containing 127 mM $H^{13}CO_2H$ and 12.7 mM **1** in CD_3CN.

The dehydrogenation of formic acid was probed using gas chromatography analysis and an inverted burette for gas evolution measurements. In one experiments, addition of formic acid to a 1 mol% solution of **2** in acetonitrile produced hydrogen in a (91% yield after heating the reaction mixture at 70 °C for 16 hours. In a separate trial, after 18 hours at 70 °C, the dehydrogenation of formic acid in the presence of 1 mol% of **2** went to 93% completion. An additional 100 equivalents of formic acid added, with respect to cobalt, added to the reaction resulted in a yield of 50% after 23 hours at 70 °C. The analysis of the kinetics of the reaction showed the rate of gas evolution increased following a slow initiation period, or lag phase (Figure 2.5). After 1.5 hours, the reaction was found to have an apparent rate constant of 2.9(3) M s^{-1} at a catalyst concentration of 12.7 mM and a zero-order dependence on formic acid. Rate constants were measured at 70, 80 and 90 °C and the relative concentrations of **2** and HCO_2H were 12.7 mM and 1.27 M respectively (Figure 2.6). Activation parameters were calculated from an Eyring plot (see Figure B1), where $\Delta H^{\ddagger}$=10(3) kcal mol^{-1} and $\Delta S^{\ddagger}$=-49(9) eu.

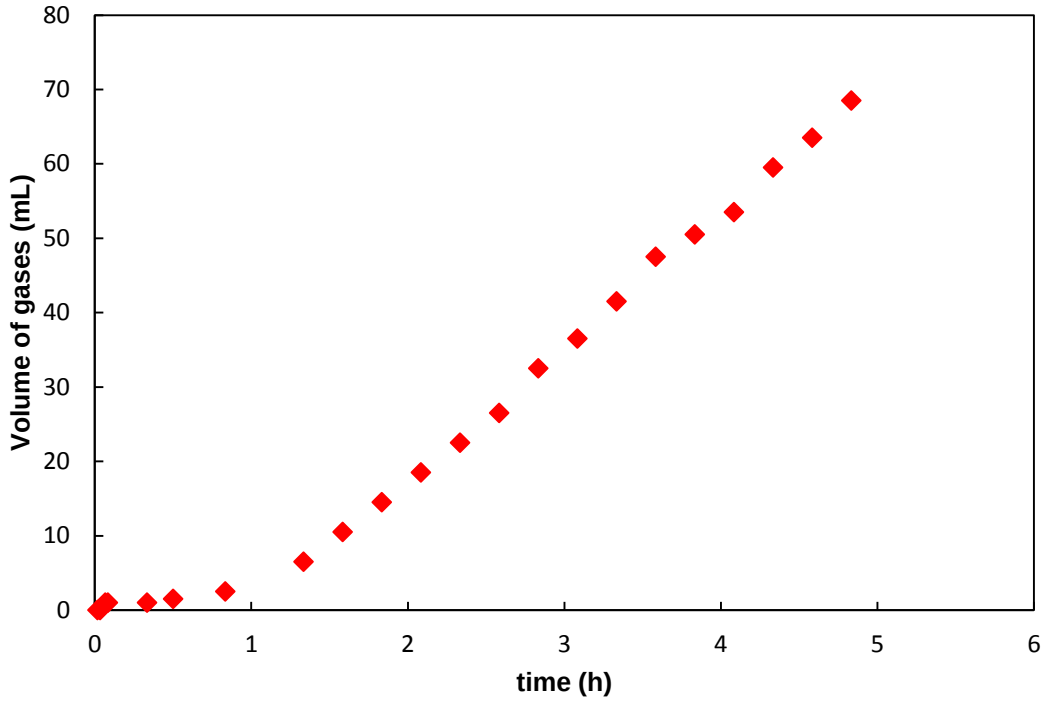

Figure 2.5. Kinetics of HCO_2H dehydrogenation in the presence of 1 mol% 1 in 1.27 mM MeCN solution at 70 °C.

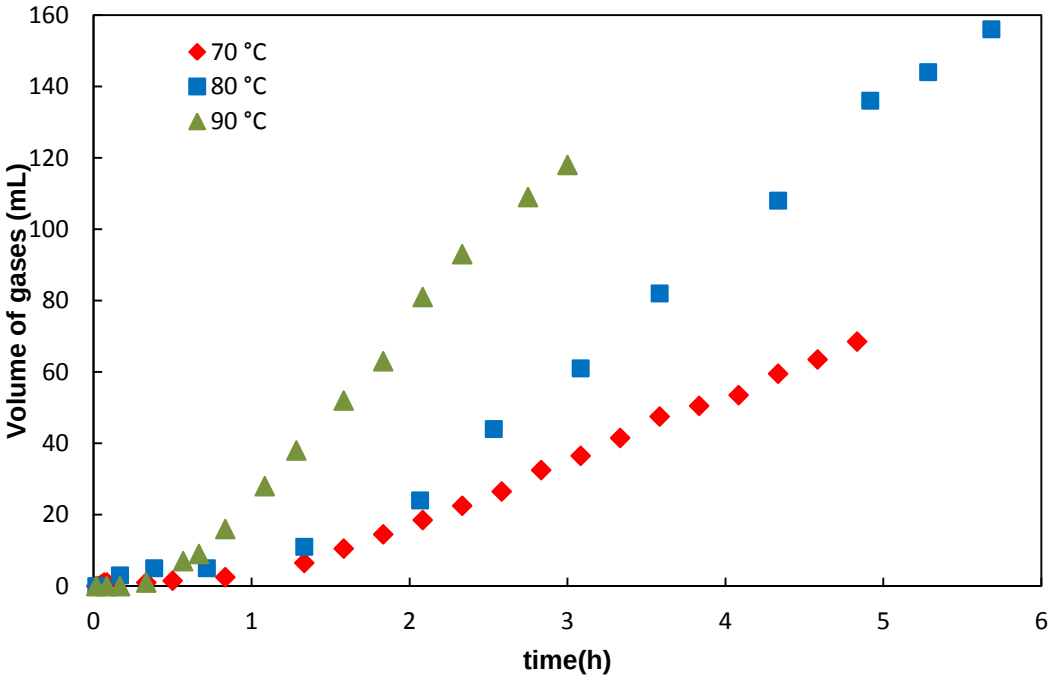

Figure 2.6. Comparison of kinetics of HCO_2H dehydrogenation 70, 80, and 90 °C.

The addition of 25.4 and 114.3 mM of triphos did not change the reaction kinetics (See B2). Furthermore, a comparison between reactions with 12.7 mM formate ([nBu$_4$N][HCO$_2$]•HCO$_2$H) and no formate at 70 °C revealed similar rate constants (Figure 2.7).

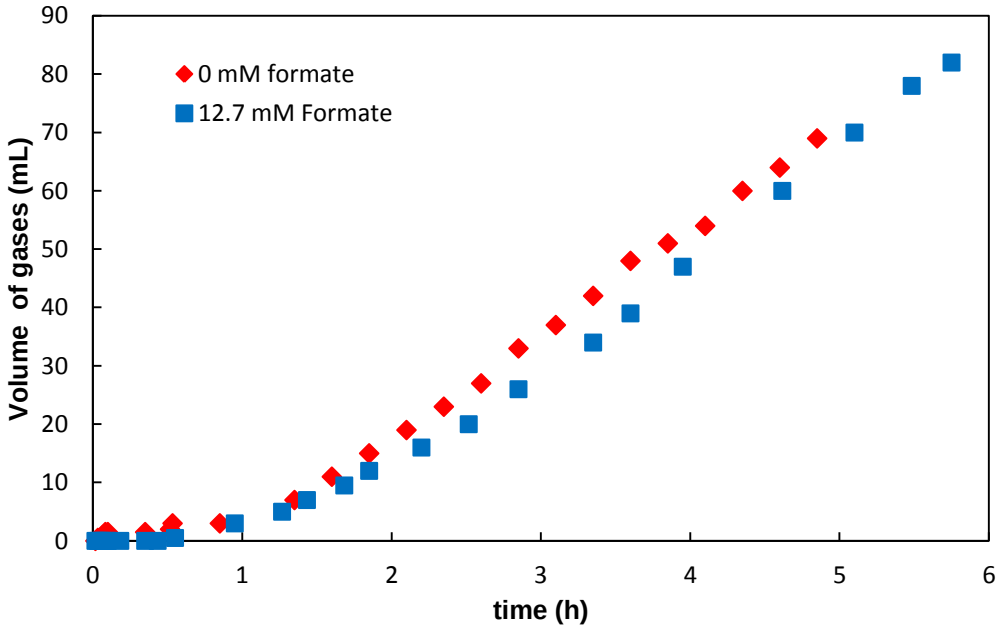

Figure 2.7. Kinetics of formic acid dehydrogenation in the presence (blue) and absence (red) of **1** mol% [nBu$_4$N][HCO$_2$]•HCO$_2$H. The solution has 12.7 mM of **1** in a 1.27 M solution of formic acid in MeCN heated to 70 °C.

Proposed Mechanism of Formic Acid Dehydrogenation

Cyclic voltammograms of **2** at a glassy carbon electrode in 1.3 mM formic acid showed enchanced current at -1.8 V vs $Fc^{+/0}$. This potential corresponds to the formation of cobalt (0) or perhaps a cobalt(II)-hydride (in the presence of acid) at the electrode (Figure 2.8). The CV suggests that hydrogen is generated by the reaction of an electrochemically derived cobalt(II)-hydride and formic acid. In the proposed mechanism, a β–hydride elimination transforms cobalt(II) formate, produced by the reaction of **2** and formic acid, to cobalt(II)-hydride. Carbon dioxide is also released in this reaction (Scheme 2.2).

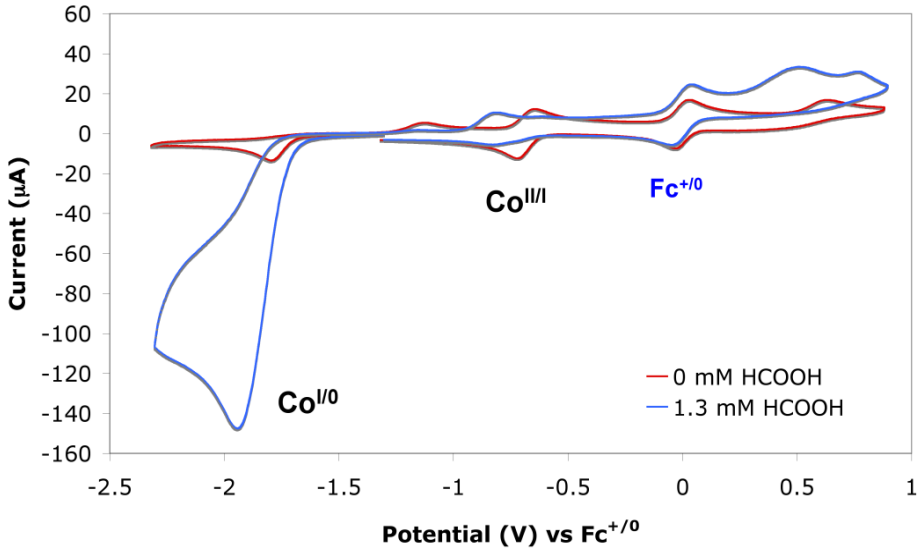

Figure 2.8. Cyclic voltammograms of **1** (0.6 mM) in acetonitrile solution containing 0.1 M [nBu$_4$N][PF$_6$] and ferrocene in the presence and absence of formic acid. Scan rate: 100 mV s^{-1}; glassy carbon electrode.

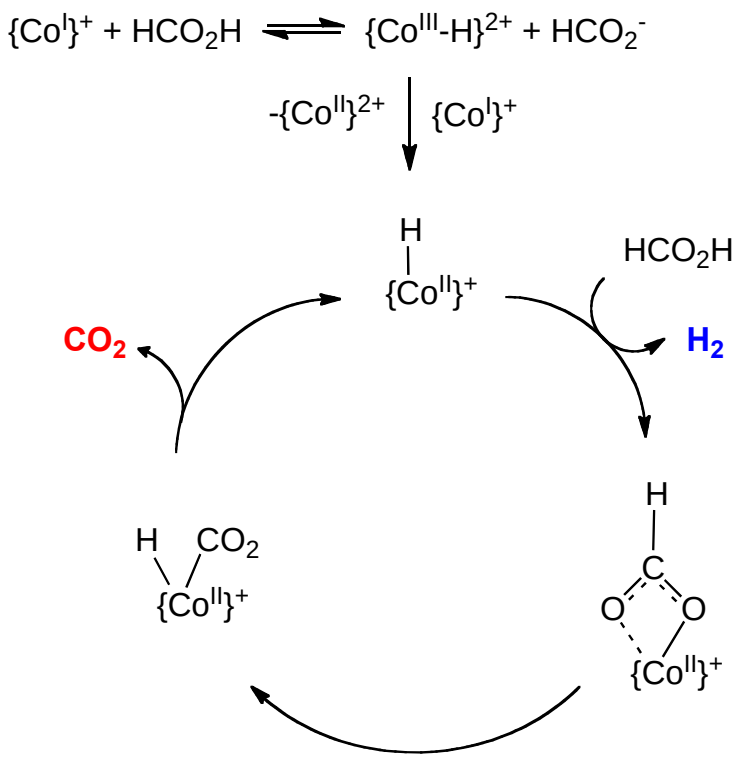

Scheme 2.2. Proposed mechanism for the dehydrogenation of formic acid.

A cobalt formate complex was isolated via the following procedure: the addition of 1 equivalent of base, $[nBu_4N][HCO_2]\bullet HCO_2H$, to a 1:1 acetonitrile:tetrahydrofuran solution of **2** resulted in an instantaneous color change of the mixture from blue to yellow. Recrystallization with diethyl ether yielded yellow crystals (Figure 2.9) that were shown by X-ray crystallography to be a cobalt(I) formate complex (**4**) (Eqn. 2.3).

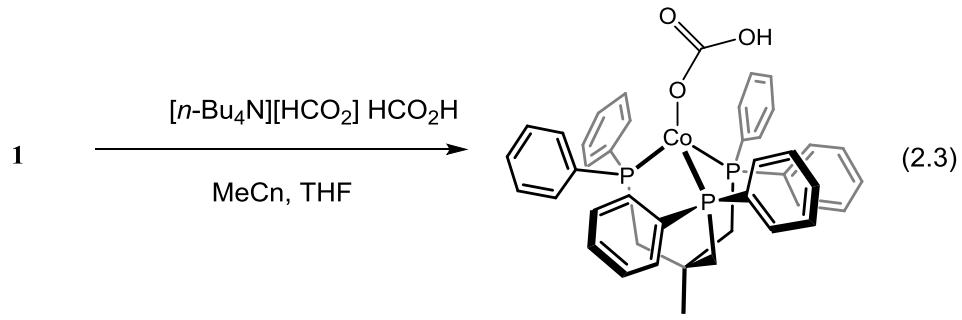

4

The Co(1)–O(1) bond length is 1.9749(17) Å; and C–O distances in the formate anion are 1.261(4) Å for O(1) and 1.224(5) Å for O(2). The Co(1)–O(2) distance is 2.977 Å (see Tables B1 and B2).

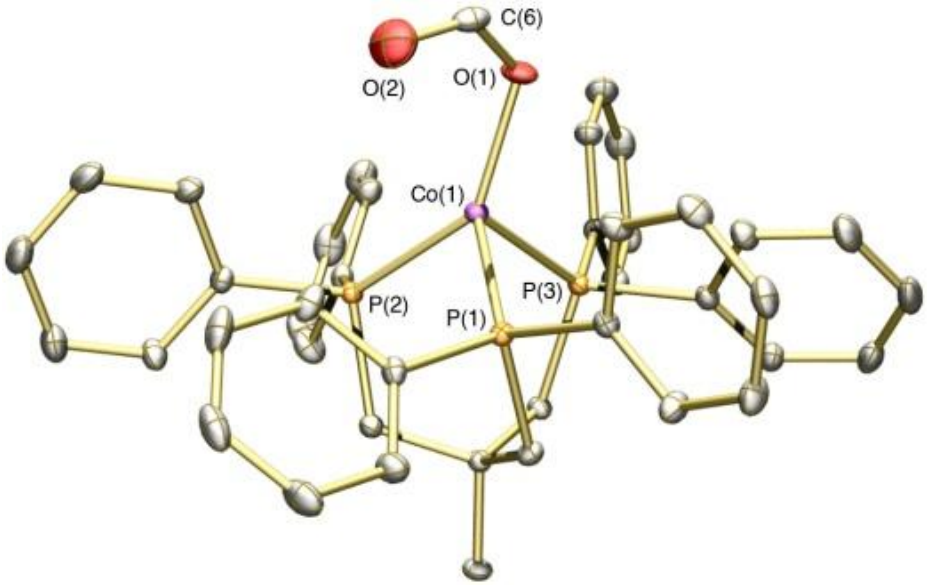

Figure 2.9. Crystal structure of **4**. Hydrogen atoms and solvent are not shown for clarity.

Kinetic Isotope Effect Studies

Kinetic isotope effect studies were conducted to further investigate the mechanism of formic acid dehydrogenation in this system. A small KIE (1-3) would indicate a rate determining X-H bond breaking step,[90] while a KIE greater than 7 would imply a direct hydride transfer resulting from a difference in the geometry of the transition state.[91, 92] The kinetic isotope effects for the reaction were measured by replacing formic acid with $HCOD_2D$, DCO_2H, and DCO_2D (Figure 1.10). The KIEs for each were 1.2(3), 1.7(3), and 2.5(3) respectively (Table 2.1). These values are similar to ones reported for the oxidation of several metal formate species that undergo β–hydride elimination. Numerical simulations of the reaction kinetics are in agreement with a mechanism that involves an initiation period, followed by a fast zero-order decay.

Table 2.1. Kinetic isotope effects.

Acid	KIE
HCO_2D	1.2(3)
DCO_2H	1.7(3)
DCO_2D	2.5(3)

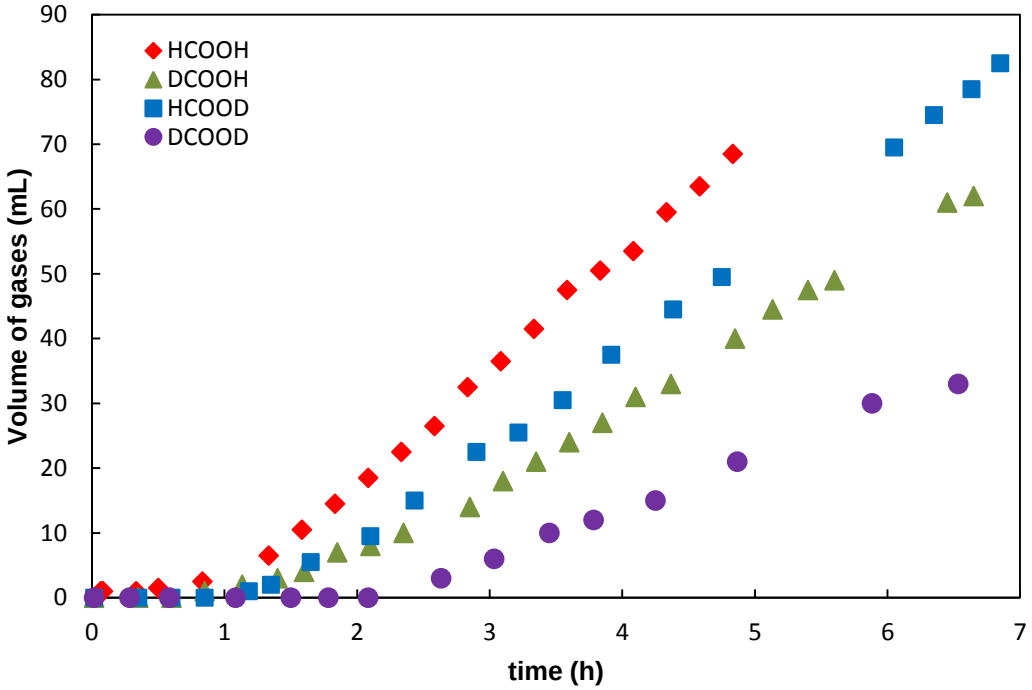

Figure 2.10. Kinetics of the dehydrogenation of HCO_2H and its deuterated variants.

Development and Synthesis of an Analogous Ligand Framework

The triphos ligand framework employed allows for facile tuning of reduction potentials as aryl groups with electron-withdrawing or electron-donating groups can be introduced. After studying the unsubstituted system in the dehydrogenation of formic acid, it was of interest to begin the investigation of analogous ligand systems. The development and synthesis of the triphos ligand with the electron donor methoxy was studied (Figure 2.11).

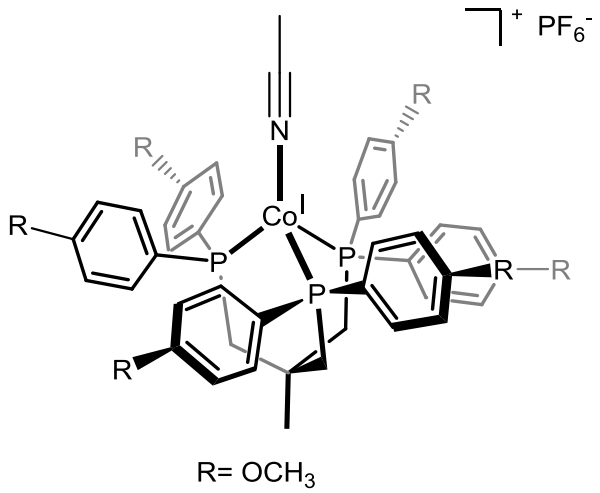

Figure 2.11. Proposed substituted cobalt species.

The ligand framework necessary to form the electron-donating cobalt catalyst is not commercially available. Syntheses adapted from literature procedures were investigated to determine the synthetic pathways that yield the desired ligand with highest purity. These syntheses may be divided into two parts: formation of a diaryl phosphine **6** or **7** and formation of the tripodal ligand **8**.

Compound **6** was synthesized following the procedure reported by Narsireddy and Yamamoto (Scheme 2.3).[93] A Grignard, formed through the reaction of 4-bromoanisole with Mg, reacts with Cl_2PNEt_2 to yield a phosphine amine in solution. The mixture was quenched with HCl and worked up in water/ethyl acetate to form the substituted phosphine oxide **5**.

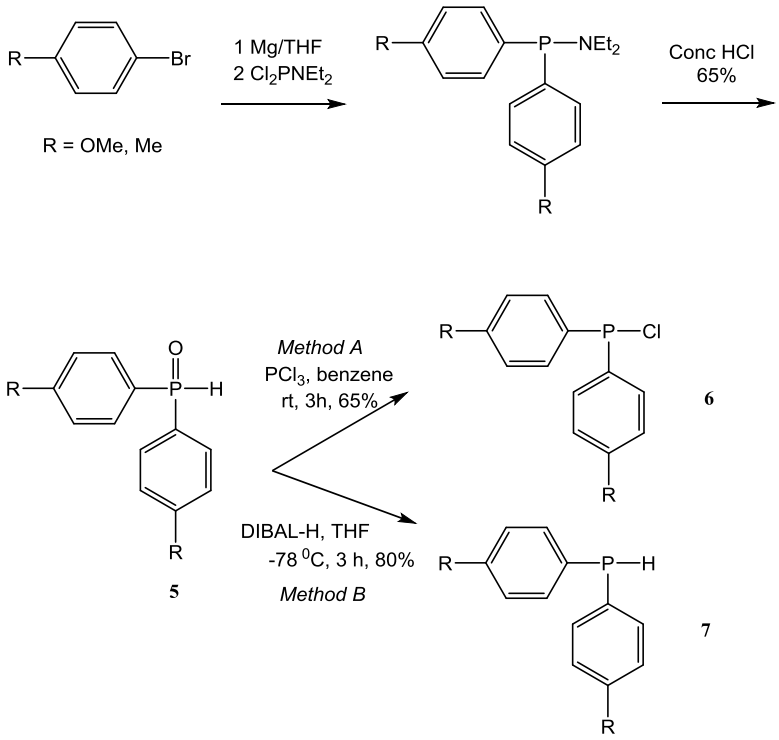

Scheme 2.3. Synthesis of R-phosphine ligand from inexpensive starting materials.

Formation of the phosphine oxide **5** was verified by NMR studies. The ^{1}H NMR spectrum displays a doublet, assigned to the P*H* group, at δ 8.19 ppm with a J_{PH} coupling constant of 480 Hz . The ^{1}H NMR spectrum also shows resonances in the 7-8 ppm region, indicative of aryl protons, and a singlet at δ 4.05 ppm, assigned as the methoxy protons, OCH_3. The ^{31}P{^{1}H} NMR spectrum exhibits only a singlet at 19.2 ppm, confirming the purity of the phosphine oxide (see Figures B3 and B4).

This phosphine oxide reacts with PCl_3 (Method A) to give **6**. The literature reported distillation under high vacuum for a related compound with a lower boiling point. However, this method was unsuccessful due to the higher boiling point of our diaryl chloro phosphine **6**.

An alternative route for the conversion from **5** to **7** was investigated, Method B (Scheme 1.3). This method is more advantageous because it does not depend on the boiling point of

the diaryl phosphine **7**, but instead relies on a series of extractions. The formation of species **7** was verified by NMR (see Figures B5 and B6).

Two methods, reported in the literature, for the formation of the triphos-OMe ligand **8** from the diaryl phosphine **7** were investigated. In Method I (Scheme 2.4), **7** reacts with 1,1,1-tris(chloromethyl)ethane in the presence of KO^{t}Bu under reflux. In Method II (Scheme 1.4), the reaction conditions include $Ni(PPh_3)_2Cl_2$ and Et_3N in DMF. Originally, both methods required purification by silica gel chromatography. However in both cases, use of silica gel led to decomposition of the product. In Method II, the resulting product was not purified through silica gel column chromatography, but passed through a short layer of silica gel. This alternative method led to product formation with 80% purity. Unfortunately, even the short silica column drastically reduced the amount of the desired product.

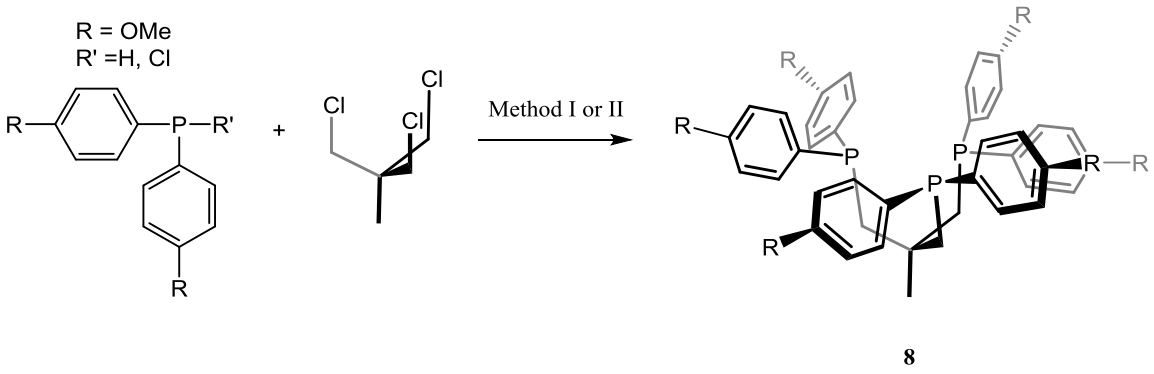

8

Scheme 2.4. Adapted syntheses of the triphos ligand frame. Reagents and conditions: *(Method I)* KO^{t}Bu, THF, reflux, 16 h; *(Method II)* $Ni(PPh_3)_2Cl_2$ (2 mol%), Et_3N, DMF, 120 ^{0}C, 12h.

Purification of the ligand was not especially effective, so the products generated through Method I and II were analyzed by NMR to determine which pathway yielded **8** with the highest purity. While both methods worked, more pure **8** was obtained from Method I. The ^{1}H NMR spectrum of the mixtures from Method I showed peaks in the aromatic region, 7-8 ppm, and peaks in the 3-4 ppm region, tentatively assigned as methoxy protons, O*CH*$_3$. Since the ^{31}P NMR spectrum of the unsubstituted ligand framework displayed a peak at

−25.2 ppm, it was expected the ligand would show a similar signal. The reaction mixture shows a signal in the ^{31}P NMR spectrum at −29.5 ppm suggesting the formation of the desired ligand.

Method I was investigated further to determine if more ideal conditions existed. Previously Method I had been carried out in THF under reflux, open to nitrogen flow. Two components of the reaction were altered: solvent system and temperature. Thus, Method I was carried out in both THF and DMSO in closed systems, sealed off from nitrogen flow. The THF was heated to 100 ^{0}C and the DMSO mixture to 150 ^{0}C. The cleanest NMR spectra were obtained from the closed system that utilized DMSO.

Preparation of a Cobalt Complex using the Analogous Ligand

GCMS of the methoxy ligands obtained from Method I have not been consistent with the expected mass of the ligand framework. **8** is expected to have a mass of 804.23 m/z or 826.23 m/z, if coordinated to sodium. However, major peaks have only been observed at 862.07 m/z and 902.8 m/z. However, these results were only from ligands purified by silica gel chromatography and, hence, are believed to be a result of decomposition of the product on silica gel.

Metallation reactions generated a metal complex using the ligands prepared from inexpensive starting materials and Methods I or II. The generated product was purified by recrystallization. Vapor diffusion of the complex in DCM with diethyl ether led to the formation of the best crystals. These crystals were suitable for X-ray crystallographic characterization. The structure obtained was surprising.

By X-ray crystallography, species **9** was observed. This complex has one dissociated phosphine and two chlorine atoms in the organic ligand (Figure 2.12). Observation of **9** could have been the result of a radical reaction. However, this seemed unlikely because it would have required the breaking of a P-C bond. More likely, the reaction of the trichloride and phosphine in Method I did not go to completion, leaving a phosphine unattached. In addition, it is suspected that use of DCM in recrystallization of the cobalt complex may

have interfered with the structure. For these two reasons, Method I was modified to make use of DMSO.

Cyclic voltammograms of **9** using a glassy carbon electrode in 0.1 M THF solution of [nBu$_4$N][PF$_6$] showed a large irreversible reduction wave near −0.357 V, which we have assigned to a $Co^{II/I}$ couple (Figure 2.13). This potential is ca. 350 mV more positive than the unsubstituted triphos complex **2**. This potential is more consistent with a rather negative CoIII/II couple in comparison with the first chapter's work. It is suspected that large peak at 1.0 V may be the oxidation of the ligand.

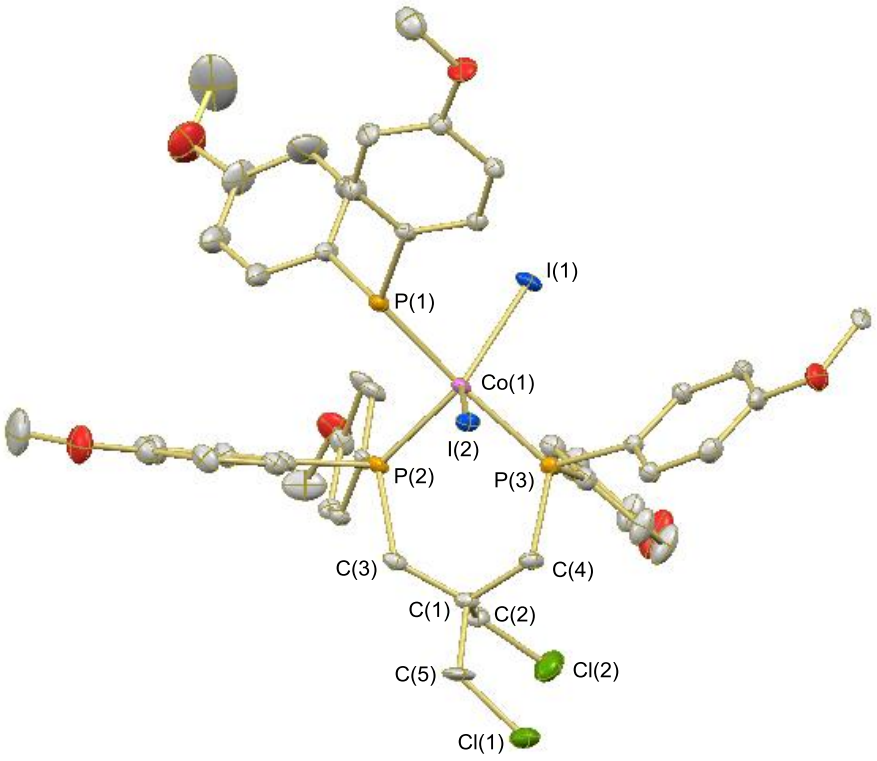

Figure 2.12. Crystallographic structure of the cobalt triphos analog complex **9.**

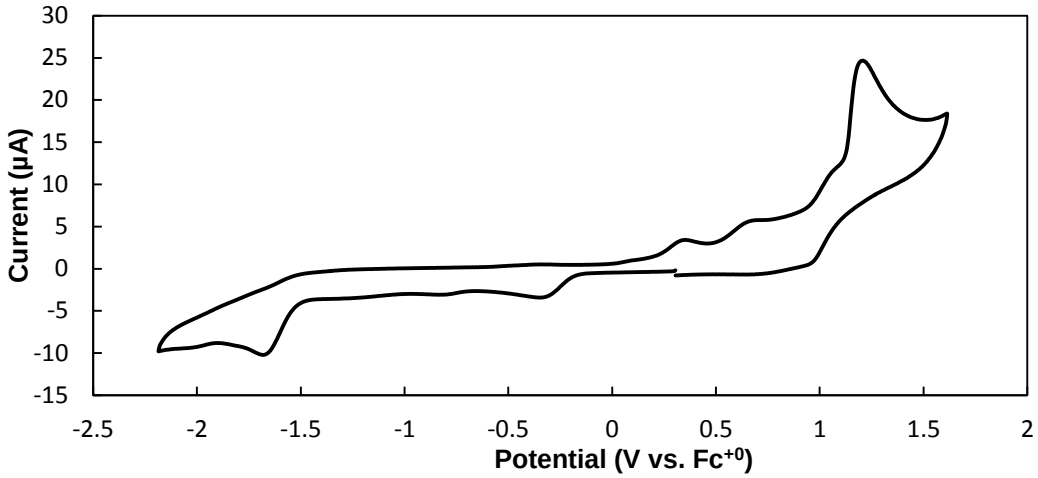

Figure 2.13. Cyclic voltammogram of the species **9** in THF.

Conclusions

In summary, formic acid can be selectively dehydrogenated in the presence of 1 mol% of a unsubstituted cobalt complex supported by a tri-phosphorus ligand framework, complex **1**. The proposed mechanism involves the formation of a cobalt(III) hydride species via protonation of cobalt(I), followed by reduction of the nascent Co^{III}-H to generate a highly reactive Co^{II}–H. Protonation of Co^{II}–H forms hydrogen and cobalt(II) formate, which upon β–hydride elimination and carbon dioxide release regenerates Co^{II}–H.

An analogue of the cobalt complex used in the dehydrogenation studies was also developed. A ligand was designed for supporting cobalt in a triphosphine ligand framework further substituted with methoxy groups on the aryl groups. The necessary intermediate, a diaryl phosphine ligand, was synthesized and subsequently reacted with KO^tBu or $Ni(PPh_3)_2Cl_2$ in order to form the desired triphos ligand. Cobalt (II) iodide was combined with one equivalent of the isolated material, yielding a cobalt (II) complex with two coordinated phosphine ligand.

R e f e r e n c e s

(1) Lewis, N. S.; Nocera, D. G. *Proc. Natl. Acad. Sci.* **2006**, *103*, 15729.

(2) Meyer, T. J. *Acc. Chem. Res.* **1989**, *22*, 163.

(3) Brudvig, G. W. *Philos. Trans. R. Soc. B Biol. Sci.* **2008**, *363*, 1211.

(4) Armstrong, F. A. *Philos. Trans. R. Soc. B Biol. Sci.* **2008**, *363*, 1263.

(5) Kamiya, N.; Shen, J.-R. *Proc. Natl. Acad. Sci.* **2003**, *100*, 98.

(6) Loll, B.; Kern, J.; Saenger, W.; Zouni, A.; Biesiadka, J. *Nature* **2005**, *438*, 1040.

(7) Ferreira, K. N. *Science* **2004**, *303*, 1831.

(8) Turner, J. A. *Science* **2004**, *305*, 972.

(9) Gray, H. B. *Nat. Chem.* **2009**, *1*, 7.

(10) Eisenberg, R.; Nocera, D. G. *Inorg. Chem.* **2005**, *44*, 6799.

(11) Vesborg, P. C. K.; Jaramillo, T. F. *RSC Adv.* **2012**, *2*, 7933.

(12) Helm, M. L.; Stewart, M. P.; Bullock, R. M.; DuBois, M. R.; DuBois, D. L. *Science* **2011**, *333*, 863.

(13) Wilson, A. D.; Shoemaker, R. K.; Miedaner, A.; Muckerman, J. T.; DuBois, D. L.; DuBois, M. R. *Proc. Natl. Acad. Sci.* **2007**, *104*, 6951.

(14) Rakowski DuBois, M.; DuBois, D. L. *Chem. Soc. Rev.* **2009**, *38*, 62.

(15) Jacques, P.-A.; Artero, V.; Pecaut, J.; Fontecave, M. *Proc. Natl. Acad. Sci.* **2009**, *106*, 20627.

(16) Connolly, P.; Espenson, J. H. *Inorg. Chem.* **1986**, *25*, 2684.

(17) Hu, X.; Cossairt, B. M.; Brunschwig, B. S.; Lewis, N. S.; Peters, J. C. *Chem. Commun.* **2005**, 4723.

(18) Hu, X.; Brunschwig, B. S.; Peters, J. C. *J. Am. Chem. Soc.* **2007**, *129*, 8988.

(19) Dempsey, J. L.; Brunschwig, B. S.; Winkler, J. R.; Gray, H. B. *Acc. Chem. Res.* **2009**, *42*, 1995.

(20) Liu, T.; Darensbourg, M. Y. *J. Am. Chem. Soc.* **2007**, *129*, 7008.

(21) Karunadasa, H. I.; Chang, C. J.; Long, J. R. *Nature* **2010**, *464*, 1329.

(22) Brown, D. E.; Mahmood, M. N.; Man, M. C. M.; Turner, A. K. *Electrochimica Acta* **1984**, *29*, 1551.

(23) Boettcher, S. W.; Warren, E. L.; Putnam, M. C.; Santori, E. A.; Turner-Evans, D.; Kelzenberg, M. D.; Walter, M. G.; McKone, J. R.; Brunschwig, B. S.; Atwater, H. A.; Lewis, N. S. *J. Am. Chem. Soc.* **2011**, *133*, 1216.

(24) McKone, J. R.; Sadtler, B. F.; Werlang, C. A.; Lewis, N. S.; Gray, H. B. *ACS Catal.* **2013**, *3*, 166.

(25) Popczun, E. J.; Read, C. G.; Roske, C. W.; Lewis, N. S.; Schaak, R. E. *Angew. Chem. Int. Ed.* **2014**, n/a.

(26) Popczun, E. J.; McKone, J. R.; Read, C. G.; Biacchi, A. J.; Wiltrout, A. M.; Lewis, N. S.; Schaak, R. E. *J. Am. Chem. Soc.* **2013**, *135*, 9267.

(27) Chen, W.-F.; Wang, C.-H.; Sasaki, K.; Marinkovic, N.; Xu, W.; Muckerman, J. T.; Zhu, Y.; Adzic, R. R. *Energy Environ. Sci.* **2013**, *6*, 943.

(28) Li, Y.; Wang, H.; Xie, L.; Liang, Y.; Hong, G.; Dai, H. *J. Am. Chem. Soc.* **2011**, *133*, 7296.

(29) Berben, L. A.; Peters, J. C. *Chem. Commun.* **2010**, *46*, 398.

(30) Krawicz, A.; Yang, J.; Anzenberg, E.; Yano, J.; Sharp, I. D.; Moore, G. F. *J. Am. Chem. Soc.* **2013**, *135*, 11861.

(31) Andreiadis, E. S.; Jacques, P.-A.; Tran, P. D.; Leyris, A.; Chavarot-Kerlidou, M.; Jousselme, B.; Matheron, M.; Pécaut, J.; Palacin, S.; Fontecave, M.; Artero, V. *Nat. Chem.* **2012**, *5*, 48.

(32) Sun, Y.; Bigi, J. P.; Piro, N. A.; Tang, M. L.; Long, J. R.; Chang, C. J. *J. Am. Chem. Soc.* **2011**, *133*, 9212.

(33) Sun, Y.; Sun, J.; Long, J. R.; Yang, P.; Chang, C. J. *Chem. Sci.* **2013**, *4*, 118.

(34) Nippe, M.; Khnayzer, R. S.; Panetier, J. A.; Zee, D. Z.; Olaiya, B. S.; Head-Gordon, M.; Chang, C. J.; Castellano, F. N.; Long, J. R. *Chem. Sci.* **2013**, *4*, 3934.

(35) King, A. E.; Surendranath, Y.; Piro, N. A.; Bigi, J. P.; Long, J. R.; Chang, C. J. *Chem. Sci.* **2013**, *4*, 1578.

(36) Kölle, U.; Grützel, M. *Angew. Chem. Int. Ed. Engl.* **1987**, *26*, 567.

(37) Schrauzer, G. N. *Acc. Chem. Res.* **1968**, *1*, 97.

(38) Kellett, R. M.; Spiro, T. G. *Inorg. Chem.* **1985**, *24*, 2373.

(39) Chao, T.-H.; Espenson, J. H. *J. Am. Chem. Soc.* **1978**, *100*, 129.

(40) Tovrog, B. S.; Kitko, D. J.; Drago, R. S. *J. Am. Chem. Soc.* **1976**, *98*, 5144.

(41) Frey, M. *ChemBioChem* **2002**, *3*, 153.

(42) Fontecilla-Camps, J. C.; Volbeda, A.; Cavazza, C.; Nicolet, Y. *Chem. Rev.* **2007**, *107*, 4273.

(43) Marr, A. *Coord. Chem. Rev.* **2001**, *219-221*, 1055.

(44) Darensbourg, M. Y.; Lyon, E. J.; Zhao, X.; Georgakaki, I. P. *Proc. Natl. Acad. Sci.* **2003**, *100*, 3683.

(45) Evans, D. J.; Pickett, C. J. *Chem. Soc. Rev.* **2003**, *32*, 268.

(46) Artero, V.; Fontecave, M. *Coord. Chem. Rev.* **2005**, *249*, 1518.

(47) Gray, H. B.; Malmström, B. G.; Williams, R. J. P. *J. Biol. Inorg. Chem.* **2000**, *5*, 551.

(48) Collman, J. P.; Wagenknecht, P. S.; Lewis, N. S. *J. Am. Chem. Soc.* **1992**, *114*, 5665.

(49) Collman, J. P.; Ha, Y.; Wagenknecht, P. S.; Lopez, M. A.; Guilard, R. *J. Am. Chem. Soc.* **1993**, *115*, 9080.

(50) Szymczak, N. K.; Berben, L. A.; Peters, J. C. *Chem. Commun.* **2009**, 6729.

(51) Valdez, C. N.; Dempsey, J. L.; Brunschwig, B. S.; Winkler, J. R.; Gray, H. B. *Proc. Natl. Acad. Sci.* **2012**, *109*, 15589.

(52) Schrauzer, G. N.; Holland, R. J. *J. Am. Chem. Soc.* **1971**, *93*, 1505.

(53) Grimes, R. N.; White, C.; Yates, A.; Maitlis, P. M. In *Inorganic syntheses. Volume 29 Volume 29*; Wiley: New York, 1992; pp. 228–234.

(54) Razavet, M.; Artero, V.; Fontecave, M. *Inorg. Chem.* **2005**, *44*, 4786.

(55) Appel, A. M.; Bercaw, J. E.; Bocarsly, A. B.; Dobbek, H.; DuBois, D. L.; Dupuis, M.; Ferry, J. G.; Fujita, E.; Hille, R.; Kenis, P. J. A.; Kerfeld, C. A.; Morris, R. H.; Peden, C. H. F.; Portis, A. R.; Ragsdale, S. W.; Rauchfuss, T. B.; Reek, J. N. H.; Seefeldt, L. C.; Thauer, R. K.; Waldrop, G. L. *Chem. Rev.* **2013**, *113*, 6621.

(56) Fukuzumi, S. *Eur. J. Inorg. Chem.* **2008**, *2008*, 1351.

(57) Weidenthaler, C.; Felderhoff, M. *Energy Environ. Sci.* **2011**, *4*, 2495.

(58) Enthaler, S. *ChemSusChem* **2008**, *1*, 801.

(59) Jiang, H.-L.; Singh, S. K.; Yan, J.-M.; Zhang, X.-B.; Xu, Q. *ChemSusChem* **2010**, *3*, 541.

(60) Grasemann, M.; Laurenczy, G. *Energy Environ. Sci.* **2012**, *5*, 8171.

(61) Johnson, T. C.; Morris, D. J.; Wills, M. *Chem. Soc. Rev.* **2010**, *39*, 81.

(62) Himeda, Y. *Green Chem.* **2009**, *11*, 2018.

(63) Boddien, A.; Federsel, C.; Sponholz, P.; Mellmann, D.; Jackstell, R.; Junge, H.; Laurenczy, G.; Beller, M. *Energy Environ. Sci.* **2012**, *5*, 8907.

(64) Kang, P.; Cheng, C.; Chen, Z.; Schauer, C. K.; Meyer, T. J.; Brookhart, M. *J. Am. Chem. Soc.* **2012**, *134*, 5500.

(65) Tanaka, R.; Yamashita, M.; Nozaki, K. *J. Am. Chem. Soc.* **2009**, *131*, 14168.

(66) Tanaka, R.; Yamashita, M.; Chung, L. W.; Morokuma, K.; Nozaki, K. *Organometallics* **2011**, *30*, 6742.

(67) Schmeier, T. J.; Dobereiner, G. E.; Crabtree, R. H.; Hazari, N. *J. Am. Chem. Soc.* **2011**, *133*, 9274.

(68) Huff, C. A.; Sanford, M. S. *ACS Catal.* **2013**, *3*, 2412.

(69) Strauss, S. H.; Whitmire, K. H.; Shriver, D. F. *J. Organomet. Chem.* **1979**, *174*, C59.

(70) King, R. B.; Bhattacharyya, N. K. *Inorganica Chim. Acta* **1995**, *237*, 65.

(71) Junge, H.; Boddien, A.; Capitta, F.; Loges, B.; Noyes, J. R.; Gladiali, S.; Beller, M. *Tetrahedron Lett.* **2009**, *50*, 1603.

(72) Shin, J. H.; Churchill, D. G.; Parkin, G. *J. Organomet. Chem.* **2002**, *642*, 9.

(73) Boddien, A.; Loges, B.; Gärtner, F.; Torborg, C.; Fumino, K.; Junge, H.; Ludwig, R.; Beller, M. *J. Am. Chem. Soc.* **2010**, *132*, 8924.

(74) Boddien, A.; Gärtner, F.; Jackstell, R.; Junge, H.; Spannenberg, A.; Baumann, W.; Ludwig, R.; Beller, M. *Angew. Chem. Int. Ed.* **2010**, *49*, 8993.

(75) Federsel, C.; Boddien, A.; Jackstell, R.; Jennerjahn, R.; Dyson, P. J.; Scopelliti, R.; Laurenczy, G.; Beller, M. *Angew. Chem. Int. Ed.* **2010**, *49*, 9777.

(76) Langer, R.; Diskin-Posner, Y.; Leitus, G.; Shimon, L. J. W.; Ben-David, Y.; Milstein, D. *Angew. Chem. Int. Ed.* **2011**, *50*, 9948.

(77) Galan, B. R.; Schöffel, J.; Linehan, J. C.; Seu, C.; Appel, A. M.; Roberts, J. A. S.; Helm, M. L.; Kilgore, U. J.; Yang, J. Y.; DuBois, D. L.; Kubiak, C. P. *J. Am. Chem. Soc.* **2011**, *133*, 12767.

(78) Federsel, C.; Ziebart, C.; Jackstell, R.; Baumann, W.; Beller, M. *Chem. - Eur. J.* **2012**, *18*, 72.

(79) Boddien, A.; Mellmann, D.; Gartner, F.; Jackstell, R.; Junge, H.; Dyson, P. J.; Laurenczy, G.; Ludwig, R.; Beller, M. *Science* **2011**, *333*, 1733.

(80) Sacconi, L.; Ghilardi, C. A.; Mealli, C.; Zanobini, F. *Inorg. Chem.* **1975**, *14*, 1380.

(81) Mealli, C.; Midollini, S.; Sacconi, L. *Inorg. Chem.* **1975**, *14*, 2513.

(82) Heinze, K.; Huttner, G.; Walter, O. *Eur. J. Inorg. Chem.* **1999**, *1999*, 593.

(83) Rupp, R.; Huttner, G.; Kircher, P.; Soltek, R.; Büchner, M. *Eur. J. Inorg. Chem.* **2000**, *2000*, 1745.

(84) Ghilardi, C. A.; Midollini, S.; Sacconi, L. *Inorg. Chem.* **1975**, *14*, 1790.

(85) Heinekey, D. M.; Liegeois, A.; van Roon, M. *J. Am. Chem. Soc.* **1994**, *116*, 8388.

(86) Mautz, J.; Heinze, K.; Wadepohl, H.; Huttner, G. *Eur. J. Inorg. Chem.* **2008**, *2008*, 1413.

(87) Winterhalter, U.; Zsolnai, L.; Kircher, P.; Heinze, K.; Huttner, G. *Eur. J. Inorg. Chem.* **2001**, *2001*, 89.

(88) Sacconi, L.; Midollini, S. *J. Chem. Soc. Dalton Trans.* **1972**, 1213.

(89) Marinescu, S. C.; Winkler, J. R.; Gray, H. B. *Proc. Natl. Acad. Sci.* **2012**, *109*, 15127.

(90) Merrifield, J. H.; Gladysz, J. A. *Organometallics* **1983**, *2*, 782.

(91) Roecker, L.; Meyer, T. J. *J. Am. Chem. Soc.* **1986**, *108*, 4066.

(92) Taylor, S. M.; Halpern, J. *J. Am. Chem. Soc.* **1959**, *81*, 2933.

(93) Narsireddy, M.; Yamamoto, Y. *J. Org. Chem.* **2008**, *73*, 9698.

A p p e n d i x A

CHAPTER 1 SUPPORTING INFORMATION

Experimental Details

General Considerations.

All solvents were of commercial grade and dried over activated alumina using a Grubbs-type solvent purification system prior to use. All chemicals were from major commercial suppliers and used without further purification. ^{1}H and ^{13}C NMR spectra were collected on 300, 400, or 500 MHz Varian spectrometers and referenced to the residual protio-solvent signal in the case of ^{1}H and ^{13}C or the deuterium lock signal in the case of ^{11}B. Chemical shifts (δ) are reported in units of ppm and coupling constants (J) are reported in Hz. Electrochemical measurements were made with a Gamry Reference 600 potentiostat/galvanostat using a standard three-electrode configuration. For all experiments, the supporting electrolyte was 0.1 M tetrabutylammonium hexafluorophosphate (Fluka, electrochemical grade) in MeCN solvent. Voltammetry collected for solution-soluble redox couples was obtained at a basal-plane graphite working electrode electrode (surface area: 0.09 cm^2). A Pt wire served as the counter electrode, with a Ag/Ag^+ reference calibrated with the ferrocene/ferrocenium couple as an external reference. Concentrations were typically 10^{-3} M.

BO_4^--bridged dimeric cobaloxime (1)

A 3-necked 500 mL round bottom flask containing H-cobaloxime (1.0 g, 3.08 mmol) was fitted with a condenser, evacuated, and put under N_2. Dry MeCN (250 mL) was cannula transferred into the setup. Trimethyl borate (1.72 mL, 15.4 mmol) was carefully syringed into the solution, followed by the addition of tetraethylammonium chloride (255 mg, 1.54 mmol). The mixture immediately changed from green to brown. After refluxing for 3 h, the solution was concentrated and cooled. The addition of diethyl ether caused a silver gray

solid to precipitate, which was filtered off. Upon drying in air, the solid turns brown. The brown solid was washed in DCM and filtered again, yielding a dark brown solid (937 mg, mmol, 70%). Upon recrystallization in MeCN/diethyl ether, a small broad peak at 20 ppm in the ^{11}B NMR disappears. ^{1}H NMR (400 MHz, MeCN-d_3) δ 18.39 (s, 1H), 3.17 (q, J = 7.2 Hz, 9H), 2.56 (s, 6H), 2.47 (s, 6H), 1.22 (t, J = 8.0 Hz, 13H). ^{13}C NMR (101 MHz, MeCN-d_3) δ 160.68 , 150.13 , 52.06 , 13.65 , 12.25 , 6.72 . ^{11}B NMR (128 MHz, MeCN-d_3) δ 7.41 .

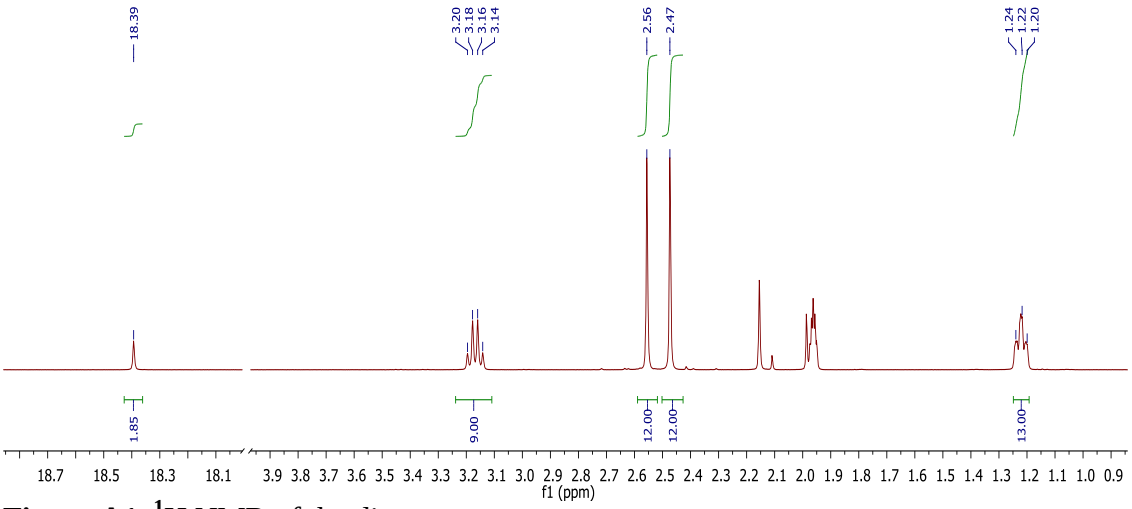

Figure A1. ^{1}H NMR of the dimer.

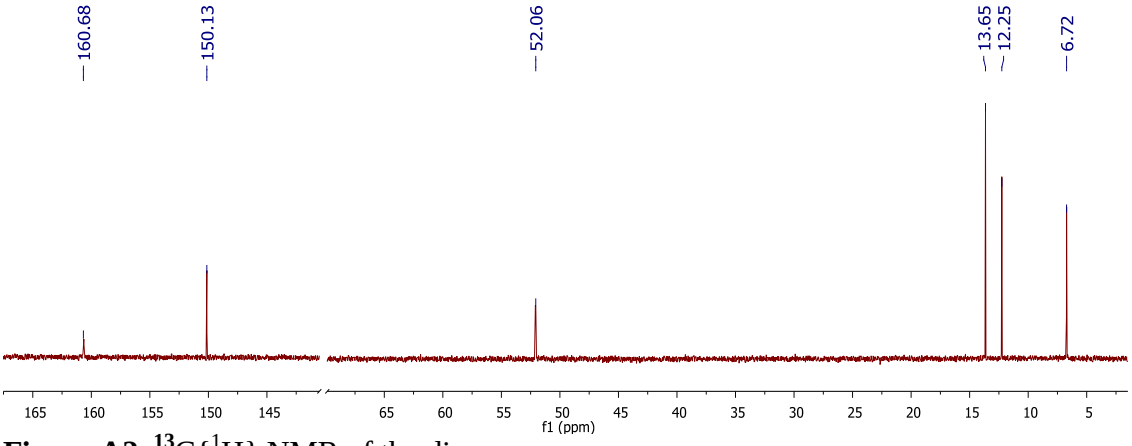

Figure A2. ^{13}C{^{1}H} NMR of the dimer.

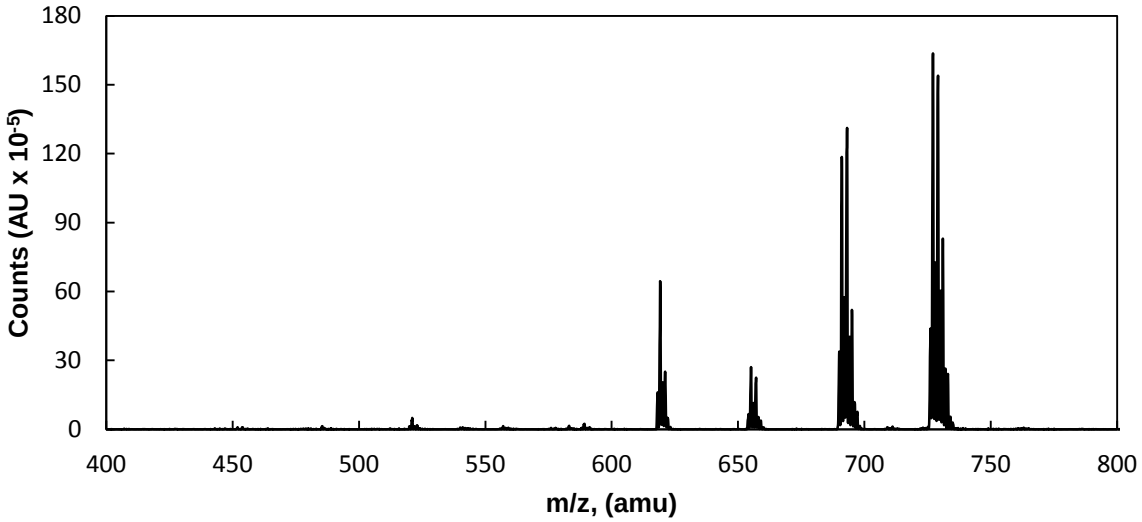

Figure A3. GCMS of complex **1** in the negative ion phase.

X-ray Structural Data

Table A1. Crystal data and structure refinement for the cobalt dimer **1**.

Chemical formula	$C_{26}\ H_{49}\ B\ Cl_4\ Co_2\ N_{10}\ O_8$
Formula weight	900.22
Crystallization solvent	Acetonitrile, diethyl ether
Crystal habit	Blade
Crystal size	0.59 x 0.27 x 0.07 mm^3
Crystal color	Brown
Data collection	
Type of diffractometer	Bruker KAPPA APEXII
Wavelength	0.71073
Data collection temperature	100(2) K
Crystal system	Triclinic
Space group	P -1
Cell dimensions	
	a = 12.5189(7) Å α = 109.121(2) °
	b = 12.7064(7) Å β = 102.053(2) °
	c = 13.0978(8) Å γ = 90.025(2) °
Cell volume	1919.77(19)
Z	2
Density (calculated)	1.557 Mg/m^3
F(000)	932
q range for data collection	1.668 to 43.747 °
Index ranges	-24≤h≤24 -24≤k≤24 -25≤l≤25
Data collection scan type	f and ω scans
Reflections collected	288113
Absorption coefficient	1.201
Max. and min. transmission	0.921 and 0.538
Refinement	
Structure solution program	XT-2014/1 (Sheldrick, 2012)
Structure refinement program	SHELXL-2014/2 (Sheldrick, 2014)
Refinement method	Full matrix least-squares on F^2
Data/restraints/parameters	29359 / 0 / 662
Goodness of fit	1.284
Final R indices[I > 2\s(I), 29359 reflections]	R1 = 0.0317, *w*R2 = 0.0716
R indices (all data)	R1 = 0.0533, *w*R2 = 0.0771
Weighting scheme	Calc $w=1/[\sigma^2Fo^2+(0.0300P)^2]$ $P=(Fo^2+2Fc^2)/3$
Max shift/error	0.004
Average shift/error	0.000
Largest diff. peak and hole	0.877 and -0.662 $Å^3$

Table A2. Selected lengths (Å) and angles (°) for the cobalt dimer **1**.

Co(1)-Co(2)	6.316(2)	Co(2)-N(8)-C(14)	116.50(5)
Co(1)-Cl(1)	2.2314(4)	Cl(1)-Co(1)-Cl(2)	176.42(2)
Co(1)-Cl(2)	2.2343(4)	Cl(1)-Co(1)-N(1)	89.44(2)
Co(1)-N(1)	1.8867(7)	Cl(1)-Co(1)-N(2)	89.42(2)
Co(1)-N(2)	1.8856(6)	Cl(1)-Co(1)-N(3)	88.36(2)
Co(1)-N(3)	1.8903(6)	Cl(1)-Co(1)-N(4)	90.67(2)
Co(1)-N(4)	1.8831(7)	Cl(2)-Co(1)-N(1)	88.24(2)
Co(2)-Cl(1)	2.2258(3)	Cl(2)-Co(1)-N(2)	92.93(2)
Co(2)-Cl(2)	2.2352(3)	Cl(2)-Co(1)-N(3)	89.32(2)
Co(2)-N(1)	1.8770(7)	Cl(2)-Co(1)-N(4)	91.70(2)
Co(2)-N(2)	1.8878(7)	N(1)-Co(1)-N(2)	81.62(3)
Co(2)-N(3)	1.8832(7)	N(1)-Co(1)-N(3)	98.89(3)
Co(2)-N(4)	1.8829(8)	N(1)-Co(1)-N(4)	178.94(3)
O(1)-N(1)	1.3343(8)	N(2)-Co(1)-N(3)	177.72(3)
O(2)-N(2)	1.3673(7)	N(2)-Co(1)-N(4)	97.32(3)
O(3)-N(3)	1.3264(8)	N(3)-Co(1)-N(4)	82.17(3)
O(4)-N(4)	1.3662(7)	Cl(3)-Co(2)-Cl(4)	178.15(2)
O(5)-N(4)	1.3648(8)	Cl(3)-Co(2)-N(5)	92.64(2)
O(6)-N(6)	1.327(1)	Cl(3)-Co(2)-N(6)	88.53(2)
O(7)-N(7)	1.3629(9)	Cl(3)-Co(2)-N(7)	93.27(2)
O(8)-N(8)	1.3384(9)	Cl(3)-Co(2)-N(8)	88.92(2)
B(1)-O(2)	1.470(1)	Cl(4)-Co(2)-N(5)	88.32(2)
B(1)-O(4)	1.4870(8)	Cl(4)-Co(2)-N(6)	90.04(2)
B(1)-O(5)	1.4747(8)	Cl(4)-Co(2)-N(7)	88.16(2)
B(1)-O(7)	1.477(1)	Cl(4)-Co(2)-N(8)	90.14(2)
		N(5)-Co(2)-N(6)	82.15(3)
Co(1)-B(1)-Co(2)	145.21(1)	N(5)-Co(2)-N(7)	97.48(3)
Co(1)-N(1)-O(1)	122.00(5)	N(5)-Co(2)-N(8)	178.31(3)
Co(1)-N(2)-O(2)	124.51(5)	N(6)-Co(2)-N(7)	178.17(3)
Co(1)-N(3)-O(3)	122.06(5)	N(6)-Co(2)-N(8)	98.55(3)
Co(1)-N(4)-O(4)	125.11(5)	N(7)-Co(2)-N(8)	81.78(3)
Co(2)-N(5)-O(5)	125.04(4)	N(2)-O(2)-B(1)	117.22(5)
Co(2)-N(6)-O(6)	122.34(5)	N(4)-O(4)-B(1)	118.64(5)
Co(2)-N(7)-O(7)	124.43(5)	N(5)-O(5)-B(1)	117.89(5)
Co(2)-N(8)-O(8)	122.22(5)	N(7)-O(7)-B(1)	118.08(5)
Co(1)-N(1)-C(1)	116.46(5)	O(2)-B(1)-O(4)	117.76(6)
Co(1)-N(2)-C(2)	116.83(5)	O(2)-B(1)-O(5)	100.01(5)
Co(1)-N(3)-C(5)	115.80(5)	O(2)-B(1)-O(7)	104.22(5)
Co(1)-N(4)-C(6)	116.15(5)	O(4)-B(1)-O(5)	104.07(5)
Co(2)-N(5)-C(9)	116.39(5)	O(4)-B(1)-O(7)	113.11(6)
Co(2)-N(6)-C(10)	115.86(5)	O(5)-B(1)-O(7)	117.54(6)
Co(2)-N(7)-C(13)	116.34(5)	O(1)-N(1)-C(1)	121.53(7)

A p p e n d i x B

CHAPTER 2 SUPPORTING INFORMATION

Experimental Details

General Considerations.

All manipulations of air and moisture sensitive materials were conducted under a nitrogen atmosphere in a Vacuum Atmospheres glovebox or on a dual manifold Schlenk line. The glassware, including NMR tubes, were oven-dried before use. Diethylether, tetrahydrofuran, dichloromethane, and acetonitrile were degassed and passed through activated alumina columns. These solvents and deuterated solvents, purchased from Cambridge Isotope Laboratories, Inc., were stored over 4 Å Linde-type molecular sieves before use. ^{1}H spectra were acquired at room temperature, unless otherwise noted, through the use of Varian spectrometers and referenced to the residual ^{1}H resonances of the deuterated solvent (^{1}H: CD_2Cl_2, δ 5.32; CD_3CN, δ 1.94). They are reported as parts per million relative to tetramethylsilane. Formic acid was dried over $CaCl_2$ for 24 hours, followed by vacuum distillation. Compounds **1**,[89] **2**,[89] and [*n*Bu_4N][HCO_2]•HCO_2H[77] were prepared according to literature procedures.

Co(triphos)(HCO_2) (4)

A THF solution (0.3 mL) of [*n*Bu_4N][HCO_2]•HCO_2H (30.3 mg, 0.0908 mmole) was added to a MeCN solution of [Co(triphos)(MeCN)][PF_6] (79 mg, 0.0908 mmole) in a 1 dram vial equipped with a magnetic stir bar. The color of the reaction mixture changed immediately from blue to yellow. The mixture was stirred at RT for 10 minutes. Vapor diffusion from diethyl ether at RT yielded yellow crystals (60 mg, 91%). Anal. Calcd for $C_{42}H_{40}CoO_2P_3$: C, 62.23; H 5.53. Found: C, 61.96; H, 5.36. X-ray quality crystals were obtained by vapor diffusion of Et2O over an MeCN solution of **3** at RT.

Cyclic voltammetry experiments

Electrochemical measurements were recorded under a nitrogen glovebox at 25 °C with a Pine Instruments WaveNow potentiostat. Electrochemical analyses were carried out in a three electrode cell consisting of a glassy carbon working electrode (surface area = 0.07 cm^2), a platinum wire counter electrode, and a silver wire reference electrode. For all measurements, the electrolyte solution was 0.1 M $[nBu_4N][PF_6]$. The ferrocene/ferrocenium couple was used to calibrate the reference electrode.

General information for kinetics experiments

In a nitrogen atmosphere glovebox, 4.0 mL of a 12.7 mM acetonitrile solution of **1** was transferred to a three neck round bottom flask equipped with a magnetic stir bar and a reflux condenser. Under a continuous flow of argon, 0.2 mL of formic acid (5.32 mmole, 1.27 M) was added to the reaction mixture. The mixture was placed in an oil bath at the desired temperature and allowed to equilibrate for 10 minutes. The volume of gases evolved was measured with an inverted burette and recorded over time.

Additional Figures

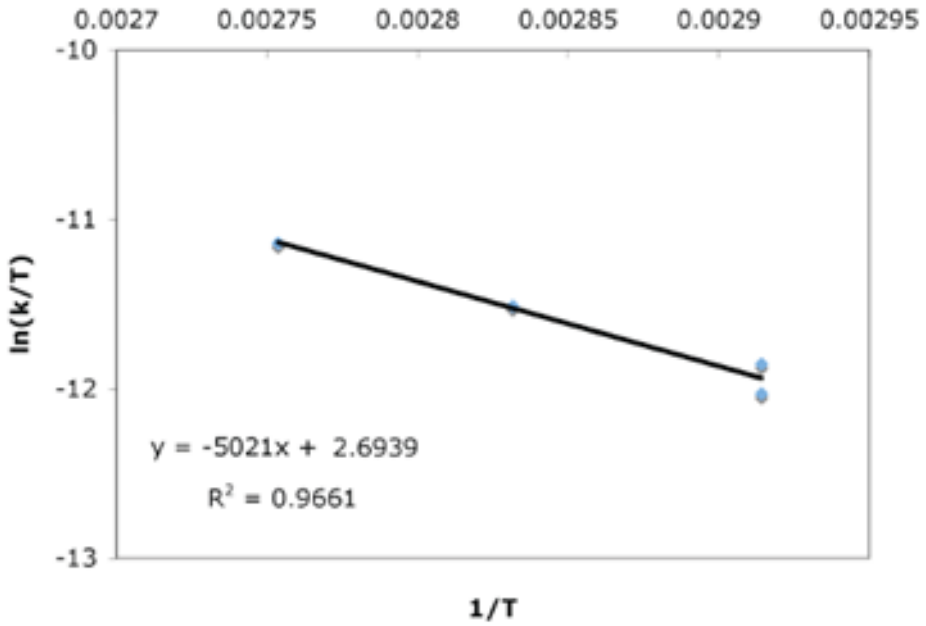

Figure B1. Eyring plot.

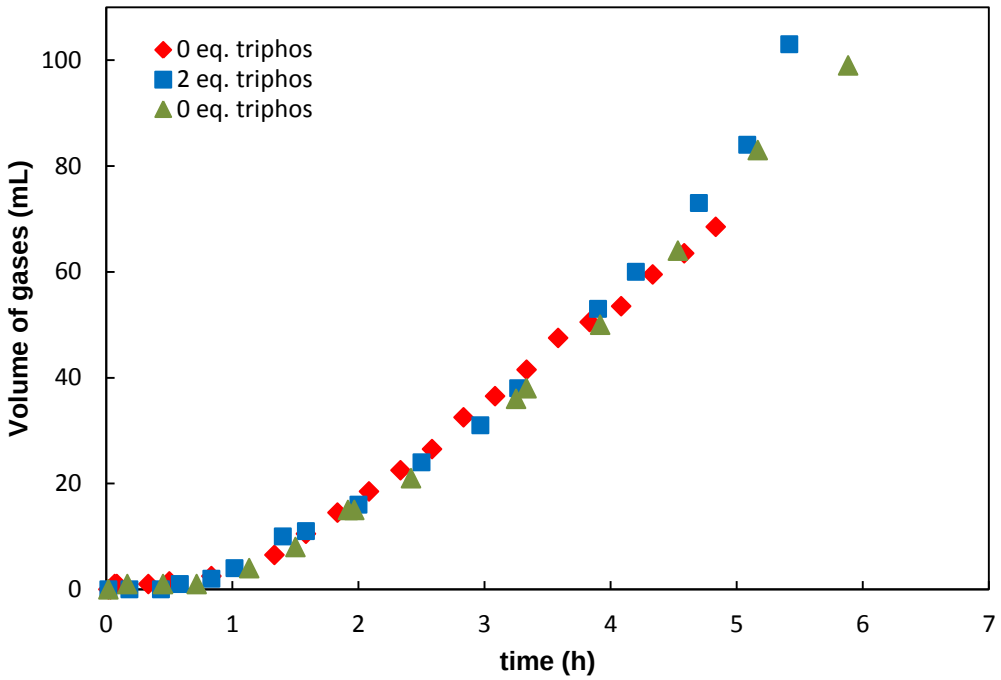

Figure B2. Dependence of the kinetics of dehydrogenation using triphos.

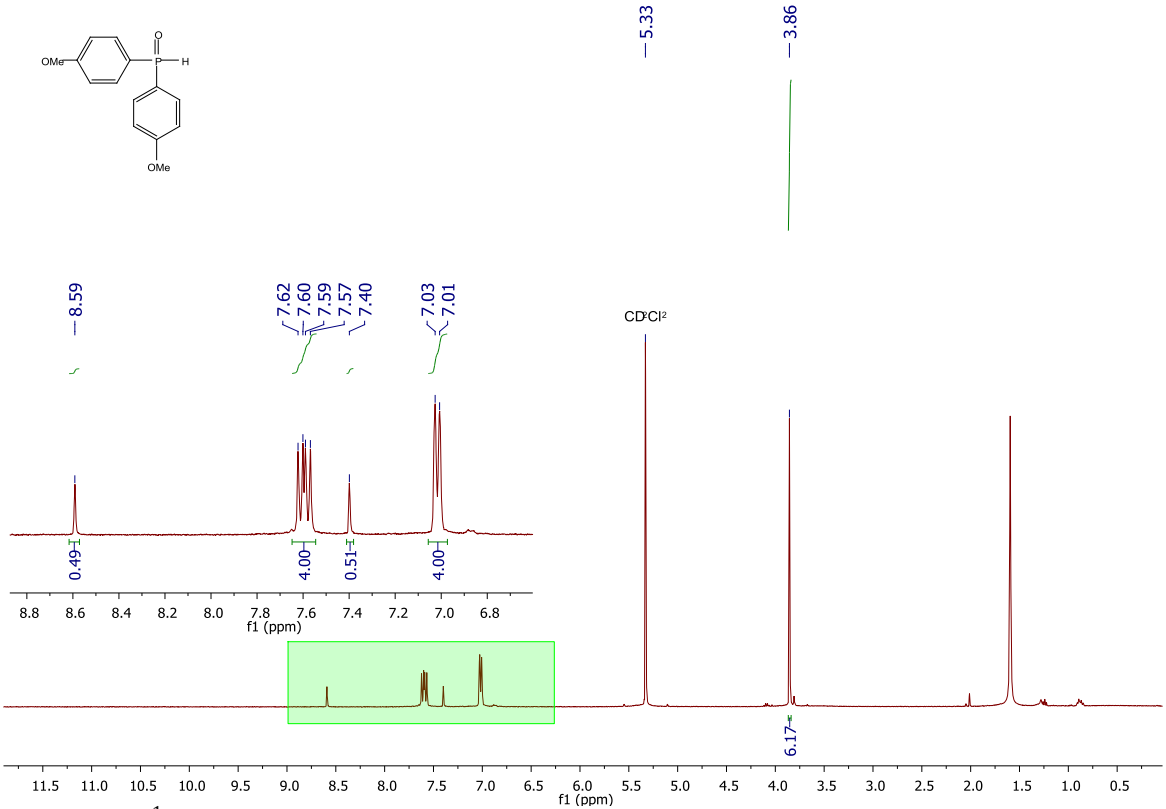

Figure B2. ^{1}H NMR spectra of the purified methoxy phosphine **5**.

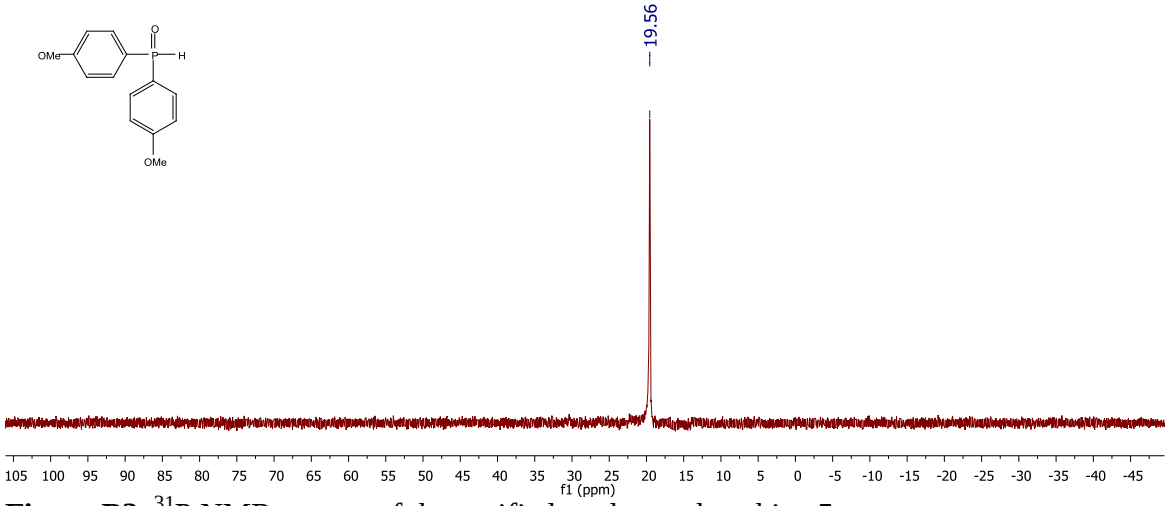

Figure B3. ^{31}P NMR spectra of the purified methoxy phosphine **5**.

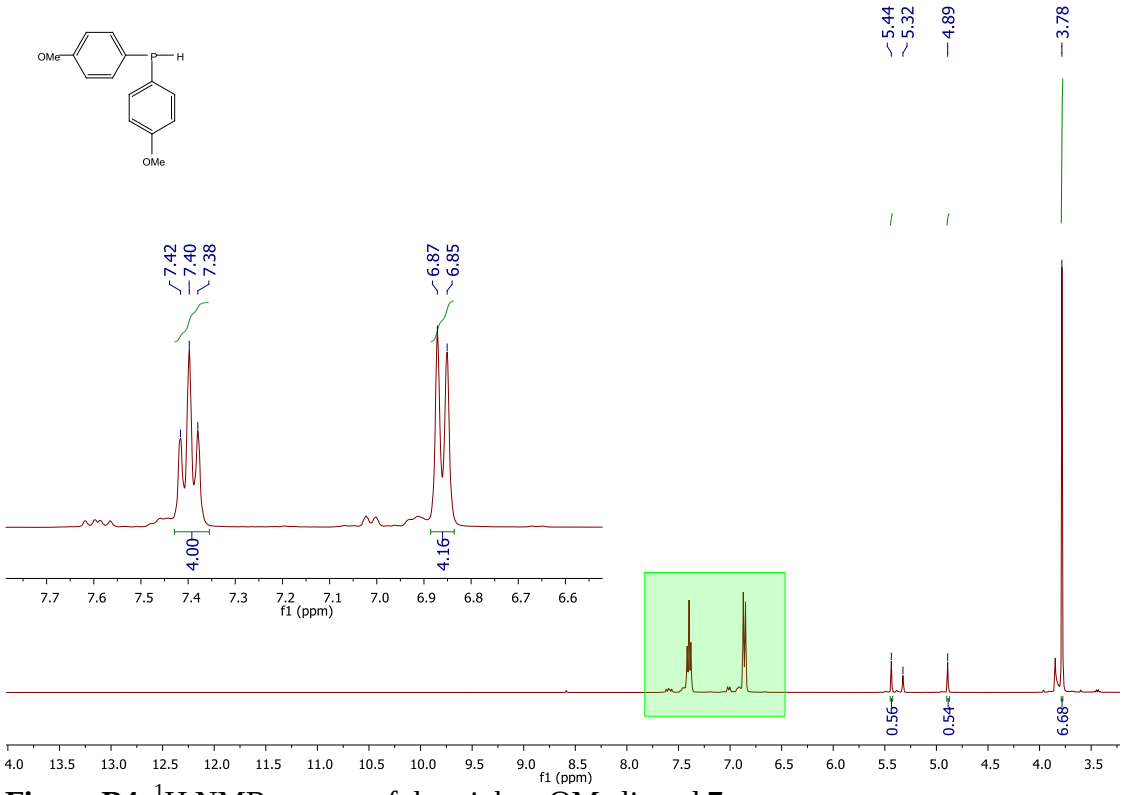

Figure B4. ^{1}H NMR spectra of the triphos-OMe ligand **7**.

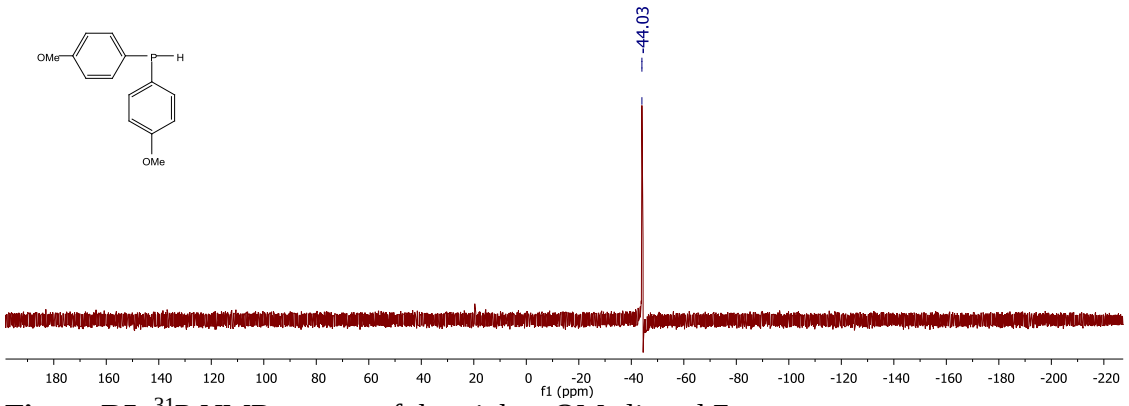

Figure B5. ^{31}P NMR spectra of the triphos-OMe ligand **7**.

X-Ray Structure Determination

Low-temperature diffraction data (and scans) were collected on a Bruker Kappa four-circle diffractometer coupled to a Bruker APEX II CCD detector with graphite monochromatedMo K radiation (=0.71073 Å) for the structure of compound **4** was solved by direct methods using SHELXS and refined against F^2 on all data by full-matrix least squares with SHELXL-2013 using established refinement techniques. All non-hydrogen atoms were refined anisotropically. All hydrogen atoms were included into the model at geometrically calculated positions and refined using a riding model. The isotropic displacement parameters of all hydrogen atoms were fixed to 1.2 times the *U* value of the atoms they are linked to (1.5 times for methyl groups). All disordered atoms were refined with the help of similarity restraints as well as rigid bond restraints on the anisotropic displacement parameters.

The cobalt formate, complex **4**, in the orthorhombic space group $Pna2_1$ with one molecule in the asymmetric unit. The formate ligand is disordered with a partially occupied chloride. This leads to a non-integral number of atoms in the unit cell.

Table B1. Crystal data and structure refinement for the cobalt formate complex **4.**

Chemical formula	$C_{41.90}\ H_{39.90}\ Cl_{10.11}\ Co\ O_{1.79}\ P_3$
Formula weight	727.57
Crystallization solvent	Acetonitrile, diethyl ether
Crystal size	0.200 x 0.200 x 0.200 mm^3
Crystal color	Yellow
Data collection	
Type of diffractometer	Bruker KAPPA APEXII
Wavelength	0.71073 Å
Data collection temperature	100(2) K
Crystal system	Orthorhombic
Space group	P n a 21
Cell dimensions	
	a = 20.7208(11) Å $\alpha = 90°$
	b = 10.0143(4) Å $\beta = 90°$
	c = 16.9376(9) Å $\gamma = 90°$
Cell volume	3514.6(3)
Z	4
Density (calculated)	1.375 Mg/m^3
F(000)	1517
q range for data collection	1.966 to 36.339 °
Index ranges	-34≤h≤31 -16≤k≤16 -28≤l≤28
Data collection scan type	f and ω scans
Reflections collected	86161
Absorption coefficient	0.669 mm^{-1}
Max. and min. transmission	0.749 and 0.657
Refinement	
Structure solution program	XT-2014/1 (Sheldrick, 2012)
Structure refinement program	SHELXL-2014/2 (Sheldrick, 2014)
Refinement method	Full matrix least-squares on F^2
Data/restraints/parameters	16896/ 49 / 444
Goodness of fit	1.039
Final R indices[I > 2\s(I), 29359 reflections]	R1 = 0.0311, *w*R2 = 0.0737
R indices (all data)	R1 = 0.0369, *w*R2 = 0.0763
Absolute structure parameter	0.001(4)
Largest diff. peak and hole	0.621 and -0.353 $Å^3$

Table B2. Selected bond lengths (Å) and angles (°) for cobalt formate complex **4**.

Co(1)-O(1)	1.9749(17)	O(1)-C(6)-O(2)	127.3(4)
Co(1)-P(1)	2.2274(4)	C(6)-O(1)-Co(1)	115.8(2)
Co(1)-P(2)	2.2331(4)	O(1)-Co(1)-P(1)	123.23(5)
Co(1)-P(2)	2.2383(4)	O(1)-Co(1)-P(2)	137.81(5)
Co(1)-Cl(1A)	2.380(7)	O(1)-Co(1)-P(3)	108.36(7)
O(1)-C(6)	1.261(4)	P(1)-Co(1)-P(2)	92.609(16)
C(6)-O(2)	1.224(5)	P(2)-Co(1)-P(3)	90.325(16)
C(6)-H(6)	0.9500	P(3)-Co(1)-P(1)	91.487(15)
C(1)-C(5)	1.535(2)	Co(1)-P(1)-C(2)	110.24(5)
C(1)-C(4)	1.545(2)	Co(1)-P(2)-C(3)	108.67(5)
C(1)-C(3)	1.553(2)	Co(1)-P(3)-C(4)	110.94(5)
C(1)-C(2)	1.555(2)	P(1)-C(2)-C(1)	114.56(11)
C(2)-P(1)	1.8473(16)	P(2)-C(3)-C(1)	116.23(10)
C(3)-P(2)	1.8501(15)	P(3)-C(4)-C(1)	114.85(10)
C(4)-P(3)	1.8467(16)	C(2)-C(1)-C(5)	107.50(11)
P(1)-C(11)	1.8260(15)	C(3)-C(1)-C(5)	106.27(12)
P(1)-C(21)	1.8354(16)	C(4)-C(1)-C(5)	107.45(13)
P(2)-C(31)	1.8350(16)	C(11)-P(1)-C(21)	98.68(7)
P(2)-C(41)	1.8415(15)	C(31)-P(2)-C(41)	100.33(7)
P(3)-C(51)	1.8257(16)	C(51)-P(3)-C(61)	99.18(7)
P(3)-C(61)	1.8339(15)		

Table B3. Crystal data and structure refinement for analog complex **9**.

Chemical formula	$C_{46}\ H_{50}\ Cl_2\ Co\ I_2\ O_6\ P_3$
Formula weight	1175.46
Crystallization solvent	Acetonitrile, diethyl ether
Crystal habit	Needles
Crystal color	Green
Data collection	
Type of diffractometer	Bruker KAPPA APEXII
Wavelength	0.71073
Data collection temperature	-173(2) K
Space group	Pbca
Cell dimensions	
	a = 20.5156(9) Å $\alpha = 90°$
	b = 18.4374(9) Å $\beta = 90°$
	c = 24.9250(13) Å $\gamma = 90°$
Cell volume	9427.99
Z	8
Density (calculated)	1.608 Mg/m^3
F(000)	4560
Index ranges	-34≤h≤234 -30≤k≤31 -41≤l≤41
Data collection scan type	f and ω scans
Reflections collected	252534
Refinement	
Structure solution program	XT-2014/1 (Sheldrick, 2012)
Structure refinement program	SHELXL-2014/2 (Sheldrick, 2014)
Refinement method	Full matrix least-squares on F^2
Data/restraints/parameters	23890 / 0 / 569
Goodness of fit	2.069
Final R indices[I > 4/s(I), 13797 reflections]	R1 = 0.0491, *w*R2 = 0.0696
R indices (all data)	R1 = 0.1011, *w*R2 = 0.0702
Weighting scheme	Calc $w=1/[\sigma^2 Fo^2]$
Max shift/error	0.020
Average shift/error	0.045
Largest diff. peak and hole	2.33 and -1.53 $Å^3$

Note that these distances are chosen to give the best fit to the X-ray data and so avoid the introduction of systematic error. The true internuclear distances are longer and do not vary with temperature! The apparent variation with temperature is caused by libration.

Table B4. Selected bond lengths (Å) and angles (°) for analog complex **9**.

Co(1)-I(1)	2.5976(1)	I(1)-Co(1)-I(2)	128.33
Co(1)-I(2)	2.6559(1)	I(1)-Co(1)-P(1)	87.67
Co(1)-P(1)	2.2381(1)	I(1)-Co(1)-P(2)	130.88
Co(1)-P(2)	2.2235(1)	I(1)-Co(1)-P(3)	91.64
Co(1)-P(3)	2.2493(1)	I(2)-Co(1)-P(1)	85.53
P(2)-C(3)	1.8445(1)	I(2)-Co(1)-P(2)	100.69
P(3)-C(4)	1.8442(1)	I(2)-Co(1)-P(3)	89.98
C(1)-C(2)	1.5311(1)	P(1)-Co(1)-P(2)	93.89
C(1)-C(3)	1.5342(1)	P(2)-Co(1)-P(3)	91.32
C(1)-C(4)	1.5320(1)	P(3)-Co(1)-P(1)	173.67
C(1)-C(5)	1.5505(1)	Co(1)-P(2)-C(3)	114.96
C(2)-Cl(2)	1.7149(1)	Co(1)-P(3)-C(4)	114.12
C(5)-Cl(1)	1.6852(1)	P(2)-C(3)-C(1)	123.56
P(1)-C(11)	1.8266(1)	P(3)-C(4)-C(1)	118.81
P(1)-C(21)	1.8140(1)	C(2)-C(1)-C(5)	108.75
P(2)-C(31)	1.8361(1)	C(3)-C(1)-C(4)	111.74
P(2)-C(41)	1.8237(1)	C(3)-C(1)-C(5)	103.49
P(3)-C(51)	1.8278(1)	C(4)-C(1)-C(5)	107.16
P(3)-C(61)	1.8260(1)	C(11)-P(1)-C(21)	102.44
		C(31)-P(2)-C(41)	103.13
		C(51)-P(3)-C(61)	101.59

INDEX